Synthesis and Characterization of a Highly Stable Amorphous Silicon Hydride

Randell L. Mills

Bala Dhandapani

Jiliang He

BlackLight Power, Inc.
493 Old Trenton Road
Cranbury, NJ 08512

A novel highly stable surface coating $SiH(1/p)$ which comprised high binding energy hydride ions was synthesized by microwave plasma reaction of mixture of silane, hydrogen, and helium wherein it is proposed that He^+ served as a catalyst with atomic hydrogen to form the highly stable hydride ions. Novel silicon hydride was identified by time of flight secondary ion mass spectroscopy and X-ray photoelectron spectroscopy. The ToF-SIMS identified the coatings as hydride by the large SiH^+ peak in the positive spectrum and the dominant H^- in the negative spectrum. XPS identified the H content of the SiH coatings as hydride ions, $H^-(1/4)$, $H^-(1/9)$, and $H^-(1/11)$ corresponding to peaks at 11, 43, and 55 eV, respectively. The silicon hydride surface was remarkably stable to air as shown by XPS. The highly stable amorphous silicon hydride coating may advance the production of integrated circuits and microdevices by resisting the oxygen passivation of the surface and possibly altering the dielectric constant and band gap to increase device performance.

I. INTRODUCTION

Aqueous *HF* acid etching of silicon surfaces results in the removal of the surface oxide and produces hydrogen terminated silicon surfaces, $Si-H$. *HF* etching is a key step in producing silicon surfaces which are contamination-free and chemically stable for subsequent processing in the semiconductor industry [1-3]. In fact, chemical oxidation and subsequent *HF* treatment of *Si* surfaces are used prior to gate oxidation, where surface contamination (<10 ppm level) and interface control are crucial to device performance. Fluorine termination was initially considered the basis of the chemical stability of *HF*-treated surfaces. Subsequently, it was found that fluorine is a minor species on the surface and that the remarkable surface passivation achieved by *HF* is explained by *H* termination of silicon dangling bonds protecting the surface from chemical attack [3, 4, 5]. However, the replacement of the oxide layer with the *H* termination of the silicon dangling bonds by *HF* can be attributed to the increased electronegativity of fluoride ion versus oxide causing an enhanced reactivity of H^+ which attacks the oxide layer. The electron affinity of halogens increases from the bottom of the Group VII elements to the top. Hydride ion may be considered a halide since it possess the same electronic structure. And, according to the binding energy trend, it should have a high binding energy. However, the binding energy is only $0.75\,eV$ which is much lower than the $3.4\,eV$ binding energy of a fluoride ion. And, once the *HF* is rinsed from the surface, the $Si-H$ layer undergoes rapid oxidation when exposed to oxygen or solvents containing oxygen. An $Si-H$ layer with enhanced stability would be of great value to the semiconductor industry.

Amorphous $Si-H$ films, the active component of important semiconductor devices such as photovoltaics, optoelectronics, and field-effect transistors are formed by plasma enhanced chemical vapor deposition (PECVD) techniques [6]. Typically the film is grown on a silicon wafer substrate exposed to a plasma of silane, hydrogen, and often argon using a reactor with a diode configuration in which the plasma is confined between two parallel electrodes. In this study, we find that the aqueous *HF* acid etched surface undergoes rapid oxidation when exposed to air and provides little protection from such exposure. Whereas, a

novel highly air stable amorphous $SiH(1/p)$ surface coating which comprised high binding energy hydride ions was synthesized by microwave plasma reaction of mixture of silane, hydrogen, and helium wherein it is proposed that He^+ served as a catalyst with atomic hydrogen to form the highly stable hydride ions. The novel amorphous $Si-H$ film may advance semiconductor fabrication and devices.

It was reported previously that a new plasma source has been developed that operates by incandescently heating a hydrogen dissociator to provide atomic hydrogen and heats a catalyst such that it becomes gaseous and reacts with the atomic hydrogen to produce a plasma called a resonance transfer or rt-plasma. It was extraordinary, that intense VUV emission was observed by Mills et al. [7] at low temperatures (e.g. $\approx 10^3\ K$) and an extraordinary low field strength of about 1-2 V/cm from atomic hydrogen and certain atomized elements or certain gaseous ions which singly or multiply ionize at integer multiples of the potential energy of atomic hydrogen, $27.2\ eV$.

Rb^+ to Rb^{2+} and $2K^+$ to $K+K^{2+}$ each provide a reaction with a net enthalpy equal to the potential energy of atomic hydrogen, $27.2\ eV$. Mills et al. have reported an energetic catalytic reaction involving a resonance energy transfer between hydrogen atoms and Rb^+ or $2K^+$ to form an rt-plasma with a very stable novel hydride ion product [8-9]. Its predicted binding energy of $3.0468\ eV$ was observed at $407.00\ nm$ with its predicted bound-free hyperfine structure lines $E_{HF} = j^2 3.0056\ X\ 10^{-5} + 3.0575\ eV$ (j is an integer) that matched for $j=1$ to $j=37$ to within a 1 part per 10^5. Furthermore, each of Cs to Cs^{2+} and Ar^+ to Ar^{2+} each provide a reaction with a net enthalpy of $27.2\ eV$. The predicted $H^-(1/2)$ ion due to hydrogen catalysis by each of K^+/K^+, Rb^+, Cs, and Ar^+ was also observed by high resolution visible spectroscopy recorded on rt-plasmas and plasma electrolysis cells at $407.00\ nm$ corresponding to its predicted binding energy of $3.0468\ eV$ [10-11]. Hydride ions with high binding energies have been observed by X-ray photoelectron spectroscopy (XPS) and by solid state magic-angle spinning proton nuclear magnetic resonance (^1H MAS NMR) having upfield shifted peaks [11-18]. Additional prior related studies that support the possibility of a novel reaction of atomic hydrogen which produces a chemically generated or assisted plasma (rt-plasma) and produces novel hydride compounds include extreme

ultraviolet (EUV) spectroscopy [7, 9, 19-31], characteristic emission from catalysis and the hydride ion products [8-11, 22-24], lower-energy hydrogen emission [19-21, 27], plasma formation [7-10, 22-26, 32-33], Balmer α line broadening [10, 20, 27-28, 34], elevated electron temperature [20, 27-28], anomalous plasma afterglow duration [32-33], power generation [18, 27, 29-30, 34-35], and analysis of chemical compounds [11-18].

The theory given previously [36-40] is based on applying Maxwell's equations to the Schrödinger equation. The familiar Rydberg equation (Eq. (1)) arises for the hydrogen excited states for $n>1$ in Eq. (2).

$$E_n = -\frac{e^2}{n^2 8\pi\varepsilon_o a_H} = -\frac{13.598\,eV}{n^2} \tag{1}$$

$$n = 1,2,3,... \tag{2}$$

An additional result is that atomic hydrogen may undergo a catalytic reaction with certain atoms and ions which singly or multiply ionize at integer multiples of the potential energy of atomic hydrogen, $m \cdot 27.2\,eV$ wherein m is an integer. The reaction involves a nonradiative energy transfer to form a hydrogen atom that is lower in energy than unreacted atomic hydrogen that corresponds to a fractional principal quantum number. That is

$$n = \frac{1}{2},\frac{1}{3},\frac{1}{4},...,\frac{1}{p};\quad p \text{ is an integer} \tag{3}$$

replaces the well known parameter $n = \text{integer}$ in the Rydberg equation for hydrogen excited states. The $n=1$ state of hydrogen and the $n = \frac{1}{\text{integer}}$ states of hydrogen are nonradiative, but a transition between two nonradiative states is possible via a nonradiative energy transfer, say $n=1$ to $n=1/2$. Thus, a catalyst provides a net positive enthalpy of reaction of $m \cdot 27.2\,eV$ (i.e. it resonantly accepts the nonradiative energy transfer from hydrogen atoms and releases the energy to the surroundings to affect electronic transitions to fractional quantum energy levels). As a consequence of the nonradiative energy transfer, the hydrogen atom becomes unstable and emits further energy until it achieves a lower-energy nonradiative state having a principal energy level given by Eqs. (1) and (3). Processes such as hydrogen molecular bond formation that occur without photons and that require collisions are

common [41]. Also, some commercial phosphors are based on resonant nonradiative energy transfer involving multipole coupling [42].

The second ionization energy of helium is $54.417\,eV$, which is equivalent to $2 \cdot 27.2\,eV$. In this case, $54.417\,eV$ is transferred nonradiatively from atomic hydrogen to He^+ which is resonantly ionized. The electron decays to the $n = 1/3$ state with the further release of $54.417\,eV$ which may be emitted as a photon. Since the products of the catalysis reaction have binding energies of $m \cdot 27.2\,eV$, they may further serve as catalysts. Thus, further catalytic transitions may occur: $n = \frac{1}{3} \rightarrow \frac{1}{4}$, $\frac{1}{4} \rightarrow \frac{1}{5}$, and so on.

The catalyst products $H(1/p)$ were predicted to be a highly reactive intermediates which further react to form a novel hydride ions $H^-(1/p)$ with predicted binding energies E_B given by the following formula [8-9, 36]:

$$E_B = \frac{\hbar^2 \sqrt{s(s+1)}}{8\mu_e a_0^2 \left[\frac{1+\sqrt{s(s+1)}}{p}\right]^2} - \frac{\pi \mu_0 e^2 \hbar^2}{m_e^2 a_0^3} \left(1 + \frac{2^2}{\left[\frac{1+\sqrt{s(s+1)}}{p}\right]^3}\right) \tag{4}$$

where p is an integer greater than one, $s = 1/2$, $\hbar$ is Planck's constant bar, μ_o is the permeability of vacuum, m_e is the mass of the electron, μ_e is the reduced electron mass, a_o is the Bohr radius, and e is the elementary charge. The ionic radius is

$$r_1 = \frac{a_0}{p}\left(1 + \sqrt{s(s+1)}\right);\ s = \frac{1}{2} \tag{5}$$

Extremely stable hydride ions may stabilize a silicon surface to unprecedented time scales to increase the yield in integrated chip fabrication. In this paper, we report the results of the reaction of silane in a helium-hydrogen microwave discharge plasma at the surface of a nickel foil. After the plasma reaction processing, the surface was analyzed by time of flight secondary ion mass spectroscopy (ToF-SIMS) and X-ray photoelectron spectroscopy (XPS).

II. EXPERIMENTAL

Synthesis

Amorphous silicon hydride ($\alpha - SiH$) films were grown on nickel substrates by their exposure to a low pressure microwave discharge of SiH_4 (2.5%)/He (96.6%)/H_2 (0.9%). The experimental set up comprising a microwave discharge cell operated under flow conditions is shown in Figure 1. The SiH_4 gas was introduced into a 1000 ml reservoir by a gas/vacuum line where it was mixed with premixed He (99%)/H_2 (1%) to obtain the reaction mixture SiH_4 (2.5%)/He (96.6%)/H_2 (0.9%) by controlling the individual gas pressures. Nickel foil (5 X 5 mm and 0.05 mm thick, Alfa Aesar 99+%) substrates were used to avoid charging during ToF-SIMS and XPS characterization. The substrates were placed inside of a quartz tube (1.3 cm in diameter by 15.5 cm long) with vacuum valves at both ends. The tube was fitted with an Opthos coaxial microwave cavity (Evenson cavity) and connected to the gas/vacuum line. The quartz tube and vacuum line were evacuated sufficiently to remove any trace moisture or oxygen. The gas mixture SiH_4 (2.5%)/He (96.6%)/H_2 (0.9%) was flowed through the quartz tube at a total pressure of 0.7 Torr maintained with a gas flow rate of 40 sccm controlled by a mass flow controller with a readout. The cell pressure was monitored by a 0-10 Torr MKS Baratron absolute pressure gauge. The microwave generator shown in Figure 1 was an Opthos model MPG-4M generator (Frequency: 2450 MHz). The microwave plasma was maintained with a 40 W (forward)/15 W (reflected) power for about 20 min. Yellow-orange coatings formed on the substrates and the wall of the quartz tube. The quartz tube was removed and transferred to a drybox with the samples inside by closing the vacuum valves at both ends and detaching the tube from the vacuum/gas line. The coated substrates were mounted on XPS and ToF-SIMS sample holders under an argon atmosphere in order to prepare samples for the corresponding analyses. One set of samples was analyzed with air exposure limited to 10 minutes and another for 20 minutes while transferring and mounting during the analyses. Separate samples were removed from the drybox and stored in air at room temperature for 48 hours or 10 days before the analyses. Controls comprised a commercial silicon wafer (Alfa Aesar 99.99%) untreated, and HF cleaned silicon wafers exposed to air for 10 minutes.

ToF-SIMS Characterization

The commercial silicon wafer, *HF* cleaned silicon wafer, and $\alpha - SiH$ coated nickel foil samples were characterized using Physical Electronics TRIFT ToF-SIMS instrument. The primary ion source was a pulsed $^{69}Ga^{+}$ liquid metal source operated at 15 keV. The secondary ions were exacted by a ± 3 keV (according to the mode) voltage. Three electrostatic analyzers (Triple-Focusing-Time-of-Flight) deflect them in order to compensate for the initial energy dispersion of ions of the same mass. The 400 pA dc current was pulsed at a 5 kHz repetition rate with a 7 ns pulse width. The analyzed area was $60\mu m$ x $60\mu m$ and the mass range was 0-1000 AMU. The total ion dose was $7X10^{11}\ ions/cm^2$, ensuring static conditions. Charge compensation was performed with a pulsed electron gun operated at 20 eV electron energy. In order to remove surface contaminants and expose a fresh surface for analysis, the samples were sputter-cleaned for 30 s using a $80\mu m$ x $80\mu m$ raster, with 600 pA current, resulting in a total ion dose of $10^{15}\ ions/cm^2$. Three different regions on each sample of $60\mu m$ x $60\mu m$ were analyzed. The positive and negative SIMS spectra were acquired. Representative post sputtering data is reported. The ToF-SIMS data were treated using 'cadence' software (Physical Electronics), which calculates the mass calibration from well-defined reference peaks.

XPS Characterization

A series of XPS analyses were made on the samples using a Scienta 300 XPS Spectrometer. The fixed analyzer transmission mode and the sweep acquisition mode were used. The angle was 15°. The step energy in the survey scan was $0.5\,eV$, and the step energy in the high resolution scan was $0.15\,eV$. In the survey scan, the time per step was 0.4 seconds, and the number of sweeps was 4. In the high resolution scan, the time per step was 0.3 seconds, and the number of sweeps was 30. $C\,1s$ at $284.5\,eV$ was used as the internal standard.

III. RESULTS AND DISCUSSION

ToF-SIMS

The positive ToF-SIMS spectra ($m/e = 0-100$) of the noncoated cleaned commercial silicon wafer and a nickel foil coated with an $\alpha - SiH$

film and exposed to air for 10 min. are shown in Figures 2 and 3, respectively. The positive ion spectrum of the control was dominated by Si^+, oxides $Si_xO_y^+$, and hydroxides $Si_x(OH)_y^+$; whereas, that of the $\alpha-SiH$ sample contained essentially no oxide or hydride peaks. Rather, it was dominated by Si^+ and a peak at $m/z=29$ which comprised a contribution from SiH^+ and $^{29}Si^+$ which were difficult to separate definitively. However, the contribution due to SiH^+ could be determined by calculating the ratio $R=\frac{^{28}Si}{^{28}SiH+^{29}Si}$. For comparison, the theoretical ratio of $\frac{^{28}Si}{^{29}Si}$ based on isotopic abundance is 19.6. R for the clean noncoated silicon wafer was 8.1. Whereas, R for the $\alpha-SiH$ sample was 1.15 indicating that the $m/z=29$ peak was overwhelmingly due to SiH^+.

The positive spectrum ($m/e=0-100$) of a nickel foil coated with an $\alpha-SiH$ film and exposed to air for 10 days before the ToF-SIMS analysis is shown in Figure 4. In this case R was 1.75 demonstrating that the sample was extraordinarily stable to air exposure. In contrast, R was 2.45 in the positive spectrum ($m/e=0-100$) of the HF cleaned silicon wafer exposed to air for only 10 min. before ToF-SIMS analysis as shown in Figure 5.

The negative ion spectra ($m/e=0-100$) of the noncoated cleaned commercial silicon wafer and a nickel foil coated with an $\alpha-SiH$ film and exposed to air for 10 min. before ToF-SIMS analysis are shown in Figures 6 and 7, respectively. The control spectrum was dominated by oxide (O^- $m/z=16$) and hydroxide (OH^- $m/z=17$); whereas, spectrum of the $\alpha-SiH$ film was dominated by hydride ion (H^- $m/z=1$). Very little oxide or hydroxide was observed.

The negative spectrum ($m/e=0-100$) of a nickel foil coated with an $\alpha-SiH$ film and exposed to air for 10 days before the ToF-SIMS analysis is shown in Figure 8. In this case, hydride ion also dominated the negative spectrum demonstrating extraordinary air stability of the $\alpha-SiH$ film. The negative spectrum ($m/e=0-100$) of the HF cleaned silicon wafer exposed to air for only 10 min. before ToF-SIMS analysis shown in Figure 9 also shows a dominant hydride as well as oxide, hydroxide, and some fluoride (F^- $m/z=19$). However, the HF treated surface was not stable with prolonged air exposure. A dominant oxide peak was observed in the negative spectrum ($m/e=0-100$) of the HF

cleaned silicon wafer exposed to air for only 3 hours before ToF-SIMS analysis as shown in Figure 10. Hydride was also observed in lesser amounts and may have resulted as a fragment of the observed hydroxide. Fluoride (F^- $m/z=19$) was also observed. The ToF-SIMS results from the *HF* treated surface is consistent with predominantly *H* termination of silicon dangling bonds as reported previously [3, 4, 5] that has undergone rapid oxidation to form mixed oxides such as *SiOH*.

These results indicate that the plasma reaction formed a highly stable hydrogenated silicon coating in the absence of fluorine observed on the *HF* treated surface. Remarkably, the $\alpha-SiH$ film was stable even after 10 days; whereas, the *HF* treated surface showed signs of oxidation over a 1500 times shorter time scale—10 mins. At 3 hours the *HF* treated surface had similarities to the control untreated silicon wafer which comprised a full oxide coating.

The plasma-reaction-formed $\alpha-SiH$ is proposed to comprise a more stable hydride ion than the *H* terminated silicon from *HF* treatment. Thus, the ion production efficiencies in ToF-SIMS analysis could be different making a comparison only qualitative and indicative of relative changes that occurred with timed air exposure. Since the *Si* $2p$ electron of all samples was equivalent except for energy shifts due to the presence of ordinary *H*, novel *H*, or oxide, qualitative analysis was possible as given in the XPS section. As shown in this section, the ToF-SIMS results were confirmed by XPS.

XPS

A survey spectrum was obtained over the region $E_b = 0\ eV$ to $1200\ eV$. The primary element peaks allowed for the determination of all of the elements present. The survey spectrum also detected shifts in the binding energies of the *Si* $2p$ peak which also identified the presence or absence of SiO_2.

The XPS survey scans of the noncoated cleaned commercial silicon wafer and a nickel foil coated with an $\alpha-SiH$ film and exposed to air for 20 min. before XPS analysis are shown in Figures 11 and 12, respectively. The major species identified in the XPS spectrum of the control sample were silicon, oxygen, and carbon; whereas, the $\alpha-SiH$ sample contained essentially silicon alone with negligible oxygen and carbon present.

The XPS spectra (96-108 eV) in the region of the $Si\,2p$ peak of the noncoated cleaned commercial silicon wafer and a nickel foil coated with an $\alpha-SiH$ film and exposed to air for 20 min. are shown in Figures 13 and 14, respectively. The XPS spectrum of the control silicon wafer shows a large SiO_2 content at 104 eV as given by Wagner et al. [45]. In contrast the $\alpha-SiH$ sample has essentially no SiO_2. In addition, spin-orbital coupling gives rise to a split $Si\,2p$ peak in pure silicon, but this peak changed to a single broad peak upon reaction to form the $\alpha-SiH$ film indicative of amorphous silicon.

The XPS spectrum (96-108 eV) in the region of the $Si\,2p$ peak of a nickel foil coated with an $\alpha-SiH$ film and exposed to air for 48 hours before the XPS analysis is shown in Figure 15. Essentially no SiO_2 was observed at 104 eV demonstrating that the sample was extraordinarily stable to air exposure. Perhaps trace $SiOH$ is present in the region of 102 eV potentially due to less than 100% coverage of the surface with the $\alpha-SiH$ film; rather, some silicon deposition may have occurred. In contrast, the XPS spectrum (96-108 eV) in the region of the $Si\,2p$ peak of the HF cleaned silicon wafer exposed to air for 10 min. before XPS analysis was essentially fully covered by partial oxides SiO_x such as $SiOH$. The mixed silicon oxide peak in the region of 101.5-104 eV shown in Figure 16 was essentially the same percentage of the $Si\,2p$ as that of the SiO_2 peak of the uncleaned wafer shown at 104 eV in Figure 13. In addition, the $O\,1s$ peak of the $\alpha-SiH$ film exposed to air for 48 hours shown in Figure 17 was negligible; whereas, that of the HF cleaned wafer exposed to air for 10 min. was intense as shown in Figure 18.

The 0-70 eV and the 0-85 eV binding energy region of high resolution XPS spectra of the commercial silicon wafer and a HF cleaned silicon wafer exposed to air for 10 min. before XPS analysis are shown in Figures 19 and 20, respectively. Only a large $O\,2s$ peak in the low binding energy region was observed in each case. The 0-70 eV binding energy region of a nickel foil coated with an $\alpha-SiH$ film and exposed to air for 20 min. before XPS analysis is shown in Figure 21. By comparison of the $\alpha-SiH$ sample to the controls, novel XPS peaks were identified at 11, 43, and 55 eV. These peaks do not correspond to any of the primary elements, silicon, carbon, or oxygen, shown in the survey scan in Figure 12, wherein the peaks of these elements are given by Wagner et al. [45].

Similarly, hydrogen is the only element which does not have primary element peaks; thus, it is the only candidate to produce the novel peaks and correspond to the H content of the SiH coatings. These peaks closely match and are assigned to hydride ions, $H^-(1/4)$, $H^-(1/9)$, and $H^-(1/11)$, respectively, given by Eqs (4-5). The novel hydride ions are proposed to form by the catalytic reaction of He^+ with atomic hydrogen and subsequent autocatalytic reactions of $H(1/p)$ to form highly stable silicon hydride products $SiH(1/p)$.

These results indicate that the plasma reaction formed a highly stable novel hydrogenated coating; whereas, the control comprised an oxide coating or an ordinary hydrogen terminated silicon surface which rapidly formed an oxide passivation layer. The hydrogen content of the $\alpha-SiH$ coating appears to be novel hydride ions with high binding energies which account for the exceptional air stability.

IV. CONCLUSIONS

Nickel substrates were coated by the reaction product of a low pressure microwave discharge plasma of SiH_4 (2.5%)/He (96.6%)/H_2 (0.9%). The ToF-SIMS identified the coatings as hydride by the large SiH^+ peak in the positive spectrum and the dominant H^- in the negative spectrum. XPS identified the H content of the SiH coatings as hydride ions, $H^-(1/4)$, $H^-(1/9)$, and $H^-(1/11)$ corresponding to peaks at 11, 43, and 55 eV, respectively. The novel hydride ions are proposed to form by the catalytic reaction of He^+ with atomic hydrogen and subsequent autocatalytic reactions of $H(1/p)$ to form highly stable silicon hydride products $SiH(1/p)$. The SiH coating was amorphous as indicated by the shape of the $Si\,2p$ peak and was remarkably stable to air exposure. After a 48 hour exposure to air, essentially no oxygen was observed as evidence by the negligible $O\,1s$ peak at 531 eV and absence of any SiO_x $Si\,2p$ peak in the region of 102-104 eV. The highly stable amorphous silicon hydride coating may advance the production of integrated circuits and microdevices by resisting the oxygen passivation of the surface and possibly altering the dielectric constant and band gap to increase device performance.

REFERENCES

1. W. Kern, Semicond. Int., April, (1984), p. 94.
2. F. J. Grunthaner, P. J. Grunthaner, Mater. Sci. Rep., Vol. 1, (1986), p. 69.
3. M. Grudner, H. Jacob, Appl. Phys. A, Vol. 39, (1986), p. 73.
4. H. Ubara, T. Imura, A. Hiraki, Solid State Comm., Vol. 50, (1984), p. 673.
5. E. Yablonovitch, D. L. Allara, C. C. Chang, T. Gmitter, T. B. Bright, Phys. Rev. Lett., Vol. 57, (1986), p. 249.
6. R. A. Street, *Hydrogenated amorphous silicon*, Cambridge University Press, Cambridge, (1991). pp. 18-61.
7. R. Mills, J. Dong, Y. Lu, "Observation of Extreme Ultraviolet Hydrogen Emission from Incandescently Heated Hydrogen Gas with Certain Catalysts", Int. J. Hydrogen Energy, Vol. 25, (2000), pp. 919-943.
8. R. L. Mills, P. Ray, "High Resolution Spectroscopic Observation of the Bound-Free Hyperfine Levels of a Novel Hydride Ion Corresponding to a Fractional Rydberg State of Atomic Hydrogen", Int. J. Hydrogen Energy, in press.
9. R. L. Mills, P. Ray, "Stationary Inverted Lyman Population Formed from Incandescently Heated Hydrogen Gas with Certain Catalysts", Chem. Phys. Letts., submitted.
10. R. Mills, P. Ray, M. Nansteel, W. Good, P. Jansson, B. Dhandapani, J. He, "Excessive Balmer α Line Broadening, Power Balance, and Novel Hydride Ion Product of Plasma Formed from Incandescently Heated Hydrogen Gas with Certain Catalysts", Int. J. Hydrogen Energy, submitted.
11. R. Mills, E. Dayalan, P. Ray, B. Dhandapani, J. He, "Highly Stable Novel Inorganic Hydrides from Aqueous Electrolysis and Plasma Electrolysis, Japanese Journal of Applied Physics, submitted.
12. R. Mills, B. Dhandapani, M. Nansteel, J. He, A. Voigt, "Identification of Compounds Containing Novel Hydride Ions by Nuclear Magnetic Resonance Spectroscopy", Int. J. Hydrogen Energy, Vol. 26, No. 9, Sept. (2001), pp. 965-979.
13. R. Mills, B. Dhandapani, N. Greenig, J. He, "Synthesis and Characterization of Potassium Iodo Hydride", Int. J. of Hydrogen Energy, Vol. 25, Issue 12, December, (2000), pp. 1185-1203.

14. R. Mills, "Novel Inorganic Hydride", Int. J. of Hydrogen Energy, Vol. 25, (2000), pp. 669-683.
15. R. Mills, "Novel Hydrogen Compounds from a Potassium Carbonate Electrolytic Cell", Fusion Technology, Vol. 37, No. 2, March, (2000), pp. 157-182.
16. R. Mills, B. Dhandapani, M. Nansteel, J. He, T. Shannon, A. Echezuria, "Synthesis and Characterization of Novel Hydride Compounds", Int. J. of Hydrogen Energy, Vol. 26, No. 4, (2001), pp. 339-367.
17. R. Mills, "Highly Stable Novel Inorganic Hydrides", Journal of New Materials for Electrochemical Systems, in press.
18. R. Mills, W. Good, A. Voigt, Jinquan Dong, "Minimum Heat of Formation of Potassium Iodo Hydride", Int. J. Hydrogen Energy, Vol. 26, No. 11, Oct., (2001), pp. 1199-1208.
19. R. Mills, P. Ray, "Spectral Emission of Fractional Quantum Energy Levels of Atomic Hydrogen from a Helium-Hydrogen Plasma and the Implications for Dark Matter", Int. J. Hydrogen Energy, Vol. 27 (3), (2002), pp. 301-322.
20. R. L. Mills, P. Ray, B. Dhandapani, J. He, "Spectroscopic Identification of Fractional Rydberg States of Atomic Hydrogen" J. Phys. Chem. Letts., submitted.
21. R. Mills, P. Ray, "Vibrational Spectral Emission of Fractional-Principal-Quantum-Energy-Level Hydrogen Molecular Ion", Int. J. Hydrogen Energy, in press.
22. R. L. Mills, P. Ray, "Spectroscopic Identification of a Novel Catalytic Reaction of Rubidium Ion with Atomic Hydrogen and the Hydride Ion Product", Int. J. Hydrogen Energy, in press.
23. R. Mills, P. Ray, Spectroscopic Identification of a Novel Catalytic Reaction of Potassium and Atomic Hydrogen and the Hydride Ion Product, Int. J. Hydrogen Energy, Vol. 27, No. 2, February, (2002), pp. 183-192.
24. R. Mills, "Spectroscopic Identification of a Novel Catalytic Reaction of Atomic Hydrogen and the Hydride Ion Product", Int. J. Hydrogen Energy, Vol. 26, No. 10, (2001), pp. 1041-1058.
25. R. Mills and M. Nansteel, "Argon-Hydrogen-Strontium Discharge Light Source", IEEE Transactions on Plasma Science, in press.

26. R. Mills, M. Nansteel, and Y. Lu, "Excessively Bright Hydrogen-Strontium Plasma Light Source Due to Energy Resonance of Strontium with Hydrogen", European Journal of Physics D, submitted.
27. R. L. Mills, P. Ray, B. Dhandapani, M. Nansteel, X. Chen, J. He, "New Power Source from Fractional Quantum Energy Levels of Atomic Hydrogen that Surpasses Internal Combustion", Spectrochimica Acta, submitted.
28. R. L. Mills, P. Ray, B. Dhandapani, J. He, "Comparison of Excessive Balmer α Line Broadening of Glow Discharge and Microwave Hydrogen Plasmas with Certain Catalysts" Chem. Phys., submitted.
29. R. Mills, J. Dong, W. Good, P. Ray, J. He, B. Dhandapani, Measurement of Energy Balances of Noble Gas-Hydrogen Discharge Plasmas Using Calvet Calorimetry, Int. J. Hydrogen Energy, in press.
30. R. Mills, M. Nansteel, and Y. Lu, "Observation of Extreme Ultraviolet Hydrogen Emission from Incandescently Heated Hydrogen Gas with Strontium that Produced an Anomalous Optically Measured Power Balance", Int. J. Hydrogen Energy, Vol. 26, No. 4, (2001), pp. 309-326.
31. R. Mills, "Observation of Extreme Ultraviolet Emission from Hydrogen-KI Plasmas Produced by a Hollow Cathode Discharge", Int. J. Hydrogen Energy, Vol. 26, No. 6, (2001), pp. 579-592.
32. R. Mills, "Temporal Behavior of Light-Emission in the Visible Spectral Range from a Ti-K2CO3-H-Cell", Int. J. Hydrogen Energy, Vol. 26, No. 4, (2001), pp. 327-332.
33. R. Mills, T. Onuma, and Y. Lu, "Formation of a Hydrogen Plasma from an Incandescently Heated Hydrogen-Catalyst Gas Mixture with an Anomalous Afterglow Duration", Int. J. Hydrogen Energy, Vol. 26, No. 7, July, (2001), pp. 749-762.
34. R. L. Mills, A. Voigt, P. Ray, M. Nansteel, B. Dhandapani, "Measurement of Hydrogen Balmer Line Broadening and Thermal Power Balances of Noble Gas-Hydrogen Discharge Plasmas", Int. J. Hydrogen Energy, in press.
35. R. Mills, N. Greenig, S. Hicks, "Optically Measured Power Balances of Anomalous Discharges of Mixtures of Argon, Hydrogen, and Potassium, Rubidium, Cesium, or Strontium Vapor", Int. J. Hydrogen Energy, in press.

36. R. Mills, *The Grand Unified Theory of Classical Quantum Mechanics*, September 2001 Edition, BlackLight Power, Inc., Cranbury, New Jersey, Distributed by Amazon.com; posted at www.blacklightpower.com.
37. R. Mills, "The Grand Unified Theory of Classical Quantum Mechanics", Global Foundation, Inc. Orbis Scientiae entitled *The Role of Attractive and Repulsive Gravitational Forces in Cosmic Acceleration of Particles The Origin of the Cosmic Gamma Ray Bursts*, (29th Conference on High Energy Physics and Cosmology Since 1964) Dr. Behram N. Kursunoglu, Chairman, December 14-17, 2000, Lago Mar Resort, Fort Lauderdale, FL, Kluwer Academic/Plenum Publishers, New York, pp. 243-258.
38. R. Mills, "The Grand Unified Theory of Classical Quantum Mechanics", Int. J. of Hydrogen Energy, in press.
39. R. Mills, "The Hydrogen Atom Revisited", Int. J. of Hydrogen Energy, Vol. 25, Issue 12, December, (2000), pp. 1171-1183.
40. R. Mills, The Nature of Free Electrons in Superfluid Helium—a Test of Quantum Mechanics and a Basis to Review its Foundations and Make a Comparison to Classical Theory, Int. J. Hydrogen Energy, Vol. 26, No. 10, (2001), pp. 1059-1096.
41. N. V. Sidgwick, *The Chemical Elements and Their Compounds*, Volume I, Oxford, Clarendon Press, (1950), p.17.
42. M. D. Lamb, *Luminescence Spectroscopy*, Academic Press, London, (1978), p. 68.
43. Microsc. Microanal. Microstruct., Vol. 3, 1, (1992).
44. For recent specifications see PHI Trift II, ToF-SIMS Technical Brochure, (1999), Eden Prairie, MN 55344.
45. C. D. Wagner, W. M. Riggs, L. E. Davis, J. F. Moulder, G. E. Mulilenberg (Editor), *Handbook of X-ray Photoelectron Spectroscopy*, Perkin-Elmer Corp., Eden Prairie, Minnesota, (1997).

Figure Captions

Figure 1. The experimental set up comprising a microwave discharge cell operated under flow conditions.

Figure 2. The positive ion ToF-SIMS spectra ($m/e = 0-100$) of a noncoated cleaned commercial silicon wafer (Alfa Aesar 99.9%).

Figure 3. The positive ion ToF-SIMS spectra ($m/e = 0-100$) of a nickel foil coated with an $\alpha-SiH$ film and exposed to air for 10 min. that showed a large SiH^+ peak.

Figure 4. The positive ion ToF-SIMS spectrum ($m/e = 0-100$) of a nickel foil coated with an $\alpha-SiH$ film and exposed to atmosphere for 10 days before the ToF-SIMS analysis that retained a large SiH^+ peak.

Figure 5. The positive ion ToF-SIMS spectrum ($m/e = 0-100$) of the *HF* cleaned silicon wafer exposed to air for 10 min. before ToF-SIMS analysis.

Figure 6. The negative ion ToF-SIMS spectrum ($m/e = 0-100$) of the noncoated cleaned commercial silicon wafer (Alfa Aesar 99.99%).

Figure 7. The negative ion ToF-SIMS spectrum ($m/e = 0-100$) of a nickel foil coated with an $\alpha-SiH$ film and exposed to air for 10 min. before ToF-SIMS analysis that was dominated by hydride ion.

Figure 8. The negative ion ToF-SIMS spectrum ($m/e = 0-100$) of a nickel foil coated with an $\alpha-SiH$ film and exposed to air for 10 days before the ToF-SIMS analysis that retained the dominant hydride ion peak.

Figure 9. The negative ion ToF-SIMS spectrum ($m/e = 0-100$) of the *HF* cleaned silicon wafer exposed to air for 10 min. before ToF-SIMS analysis.

Figure 10. The negative ion ToF-SIMS spectrum ($m/e = 0-100$) of the *HF* cleaned silicon wafer exposed to air for 3 hours before ToF-SIMS analysis showing a dominant oxide peak.

Figure 11. The XPS survey scan of the noncoated cleaned commercial silicon wafer showing a large amount of oxide and carbon contamination of the surface.

Figure 12. The XPS survey scan of a nickel foil coated with an $\alpha-SiH$ film and exposed to air for 20 min. before XPS analysis showing minimal oxide and carbon.

Figure 13. The XPS spectrum (96-108 eV) in the region of the *Si 2p* peak of the noncoated cleaned commercial silicon wafer showing a large SiO_2 in the region of 104 eV.

Figure 14. The XPS spectrum (96-108 eV) in the region of the *Si 2p* peak of a nickel foil with an $\alpha - SiH$ film and exposed to air for 20 min. before XPS analysis showing no oxide in the region of 104 eV.

Figure 15. The XPS spectrum (96-108 eV) in the region of the *Si 2p* peak of a nickel foil coated with an $\alpha - SiH$ film and exposed to air for 48 hours before the XPS analysis showing no oxide at 104 eV and possibly trace *SiOH* in the region of 102 eV.

Figure 16. The XPS spectrum (96-108 eV) in the region of the *Si 2p* peak of the *HF* cleaned silicon wafer exposed to air for 10 min. before XPS analysis showing a very large SiO_x peak in the region of 101.5-104 eV.

Figure 17. The XPS spectrum (525-540 eV) in the region of the *O 1s* peak of a nickel foil coated with an $\alpha - SiH$ film and exposed to air for 48 hours before XPS analysis showing a minimal amount of oxide.

Figure 18. The XPS spectrum (525-540 eV) in the region of the *O 1s* peak of the *HF* cleaned silicon wafer exposed to air for 10 min. before XPS analysis showing a very large oxide peak.

Figure 19. The 0-70 eV binding energy region of a high resolution XPS spectrum of the commercial silicon wafer showing only a large *O 2s* peak in the low binding energy region.

Figure 20. The 0-85 eV binding energy region of a high resolution XPS spectrum of the *HF* cleaned silicon wafer exposed to air for 10 min. before XPS analysis showing only a large *O 2s* peak in the low binding energy region.

Figure 21. The 0-70 eV binding energy region of a high resolution XPS spectrum of a nickel foil coated with an $\alpha - SiH$ film and exposed to air for 20 min. before XPS analysis. The novel peaks observed at 11, 43 and 55 eV which could not be assigned to the elements identified by their primary XPS peaks matched and were assigned to $H^-(1/4)$, $H^-(1/9)$, and $H^-(1/11)$. The novel highly stable hydride ions formed by the catalytic reaction of He^+ and atomic hydrogen may be the basis of the extraordinary stability of the $\alpha - SiH$ film.

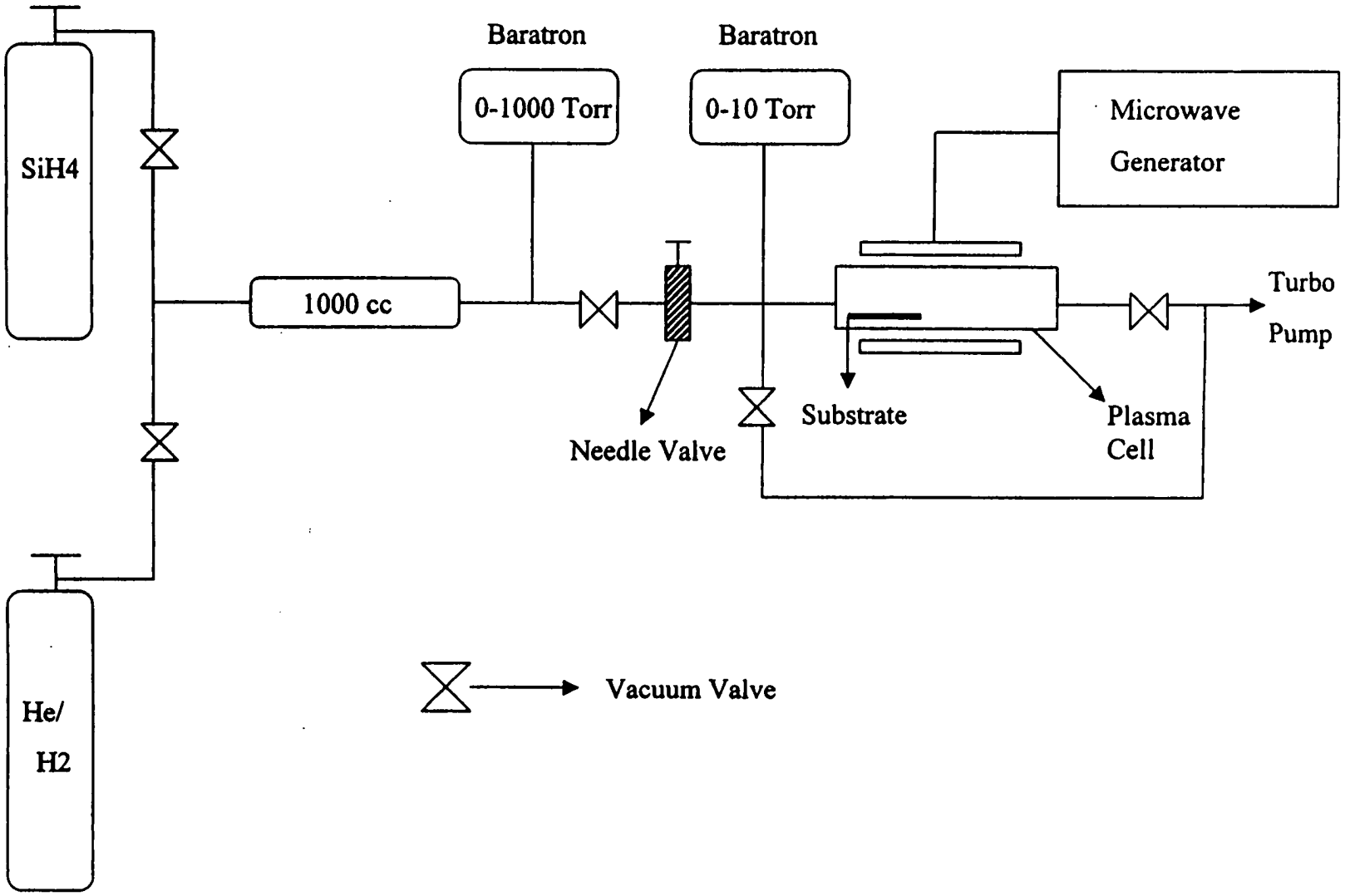
Baratron
Baratron
0-1000 Torr
0-10 Torr
Microwave
Generator
SiH4
1000 cc
Turbo
Pump
Needle Valve
Substrate
Plasma
Cell
He/
H2
Vacuum Valve

Fig. 1

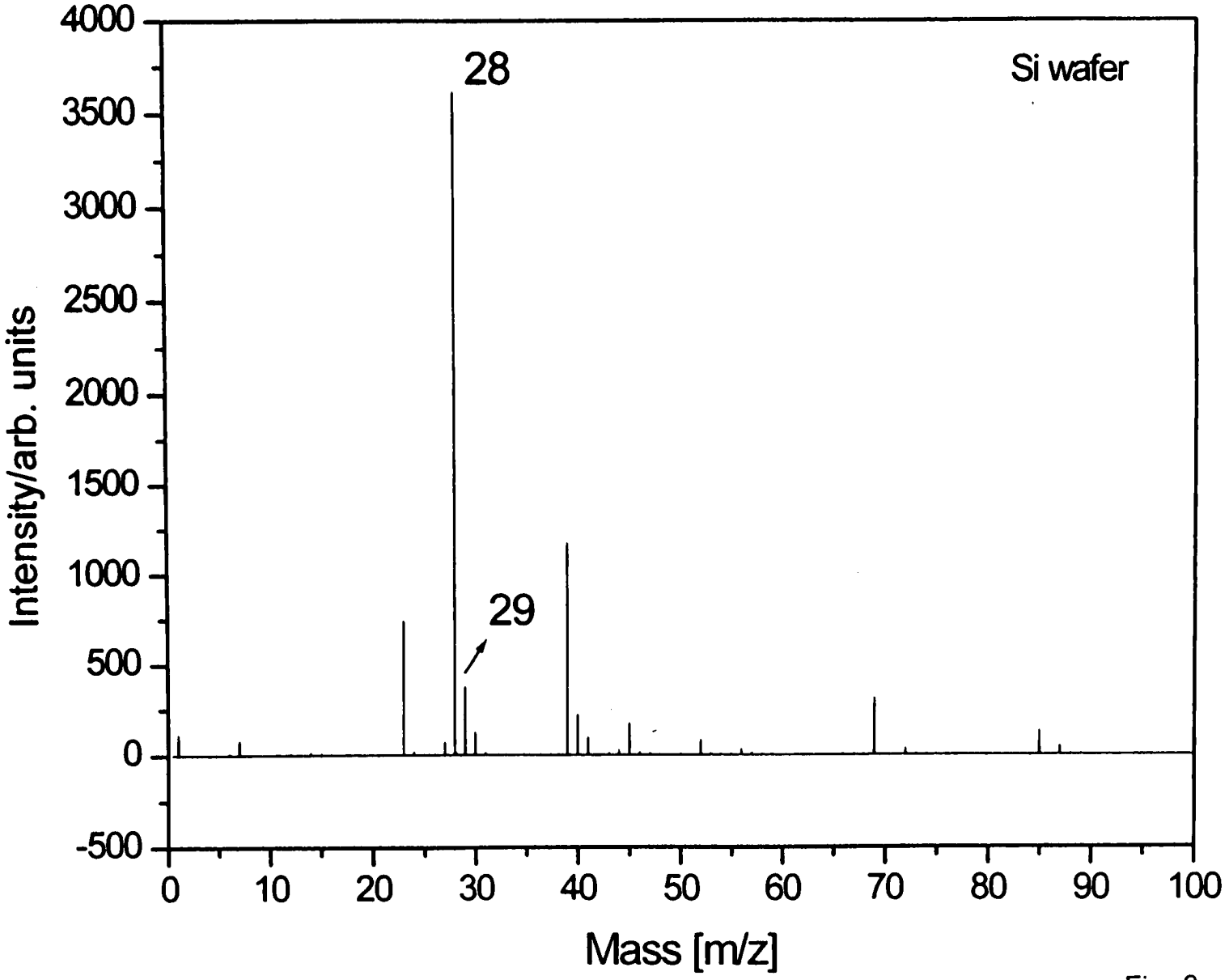
4000
3500
3000
2500
2000
1500
1000
500
0
-500
Intensity/arb. units
28
29
Si wafer
0
10
20
30
40
50
60
70
80
90
100
Mass [m/z]

Fig. 2

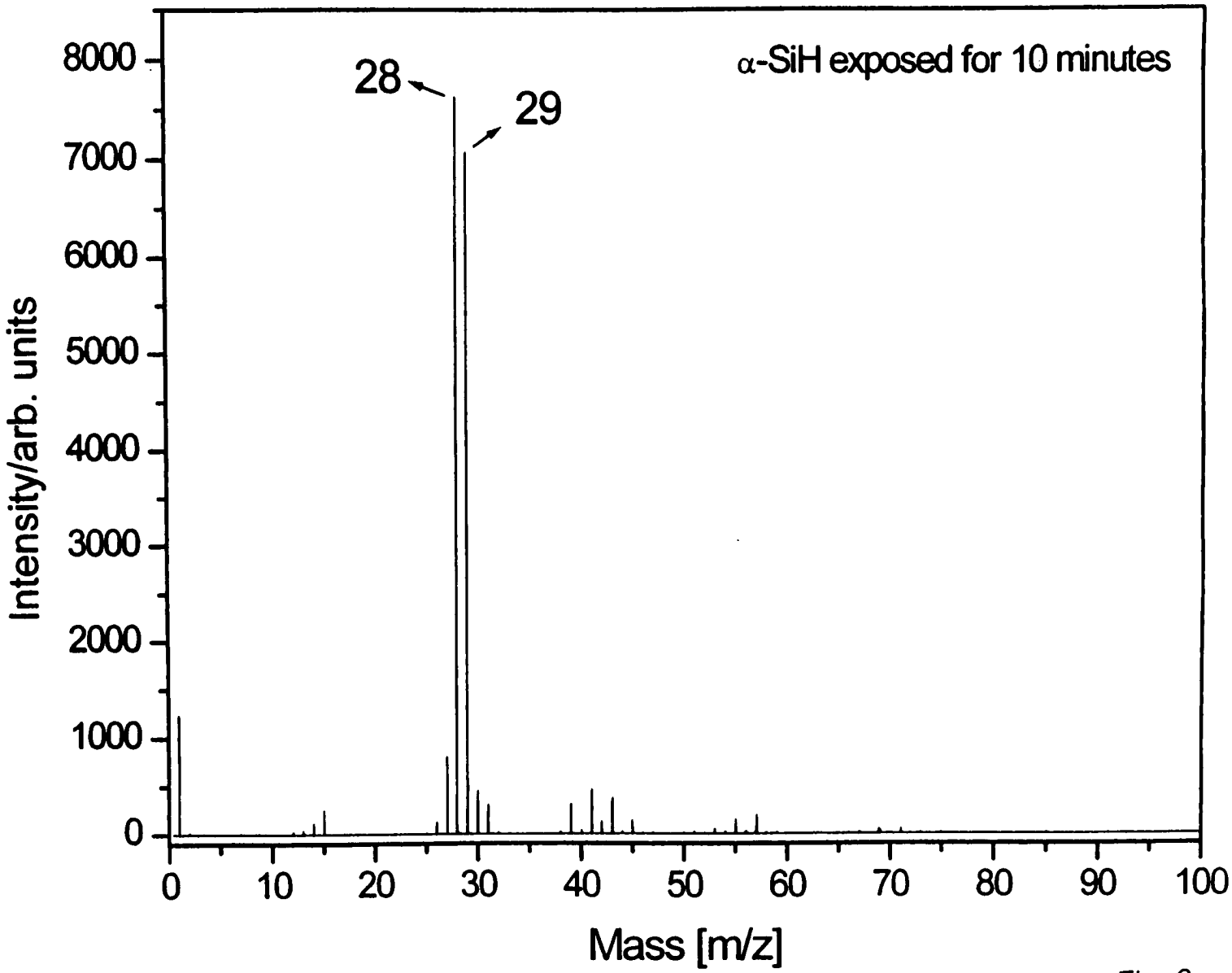
α-SiH exposed for 10 minutes
28
29
Intensity/arb. units
8000
7000
6000
5000
4000
3000
2000
1000
0
0
10
20
30
40
50
60
70
80
90
100
Mass [m/z]

Fig. 3

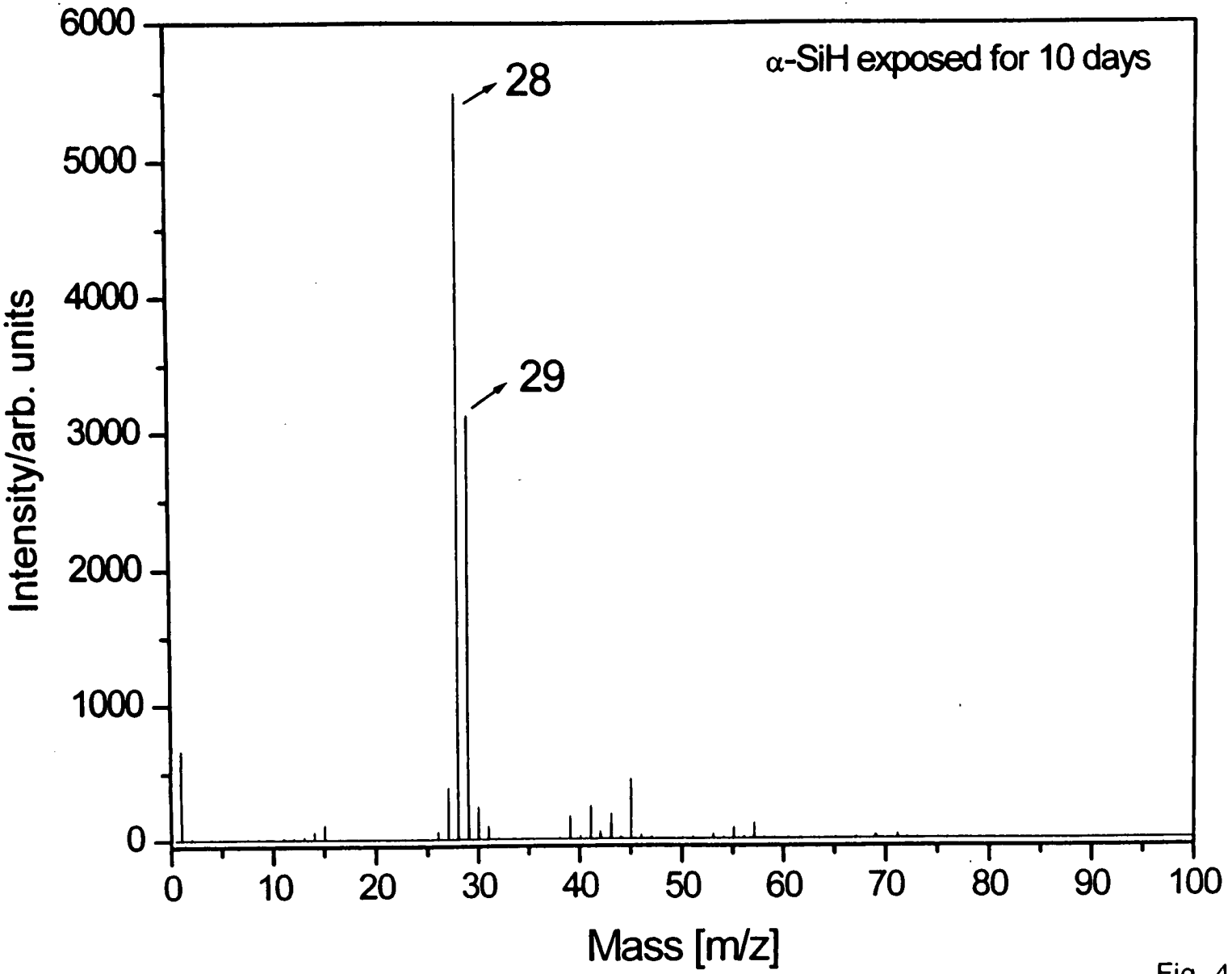
α-SiH exposed for 10 days
28
29
Intensity/arb. units
Mass [m/z]
6000
5000
4000
3000
2000
1000
0
0
10
20
30
40
50
60
70
80
90
100

Fig. 4

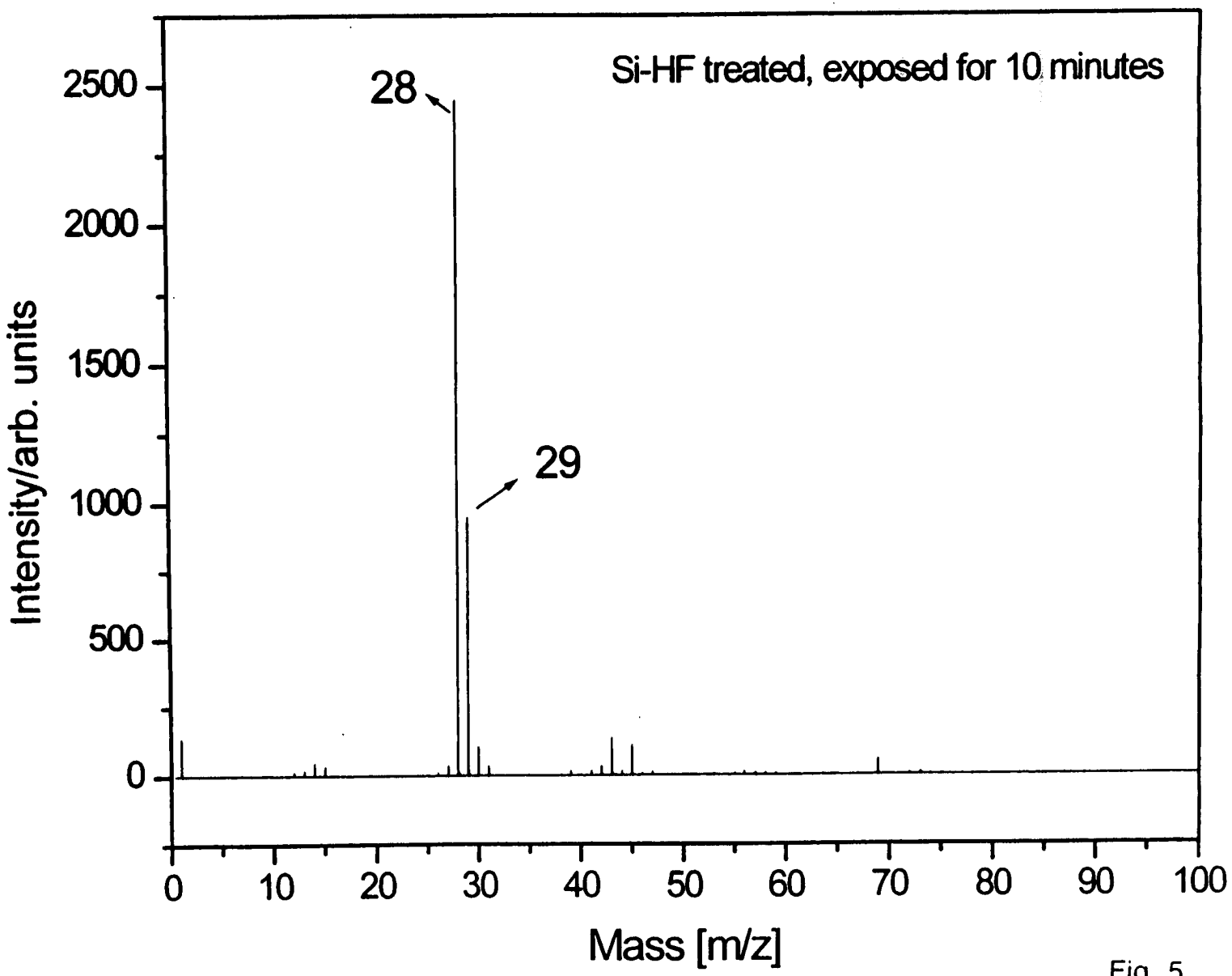
Si-HF treated, exposed for 10 minutes
28
29
Intensity/arb. units
2500
2000
1500
1000
500
0
0
10
20
30
40
50
60
70
80
90
100
Mass [m/z]

Fig. 5

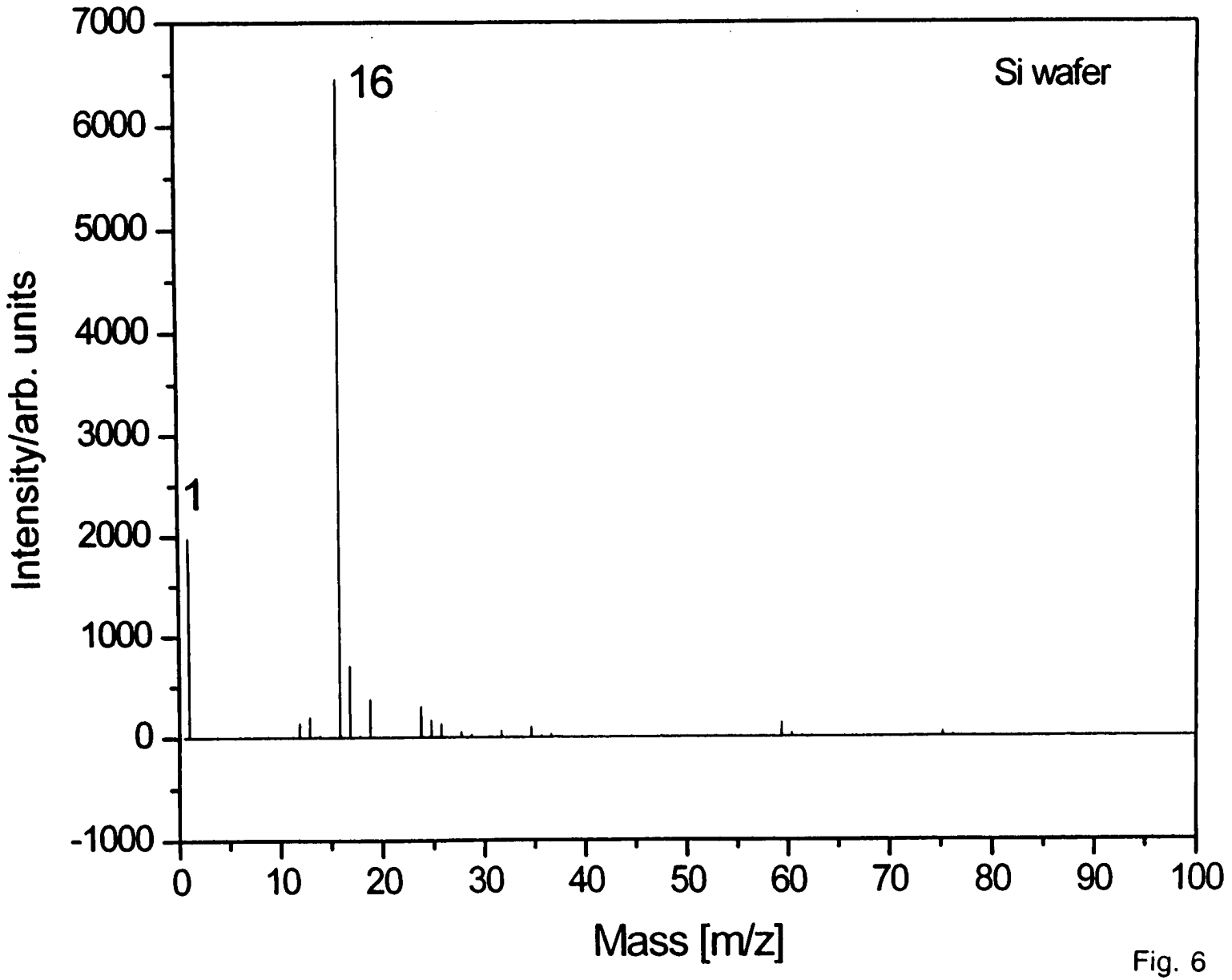
7000
6000
5000
4000
3000
2000
1000
0
-1000
Intensity/arb. units
16
1
Si wafer
0
10
20
30
40
50
60
70
80
90
100
Mass [m/z]

Fig. 6

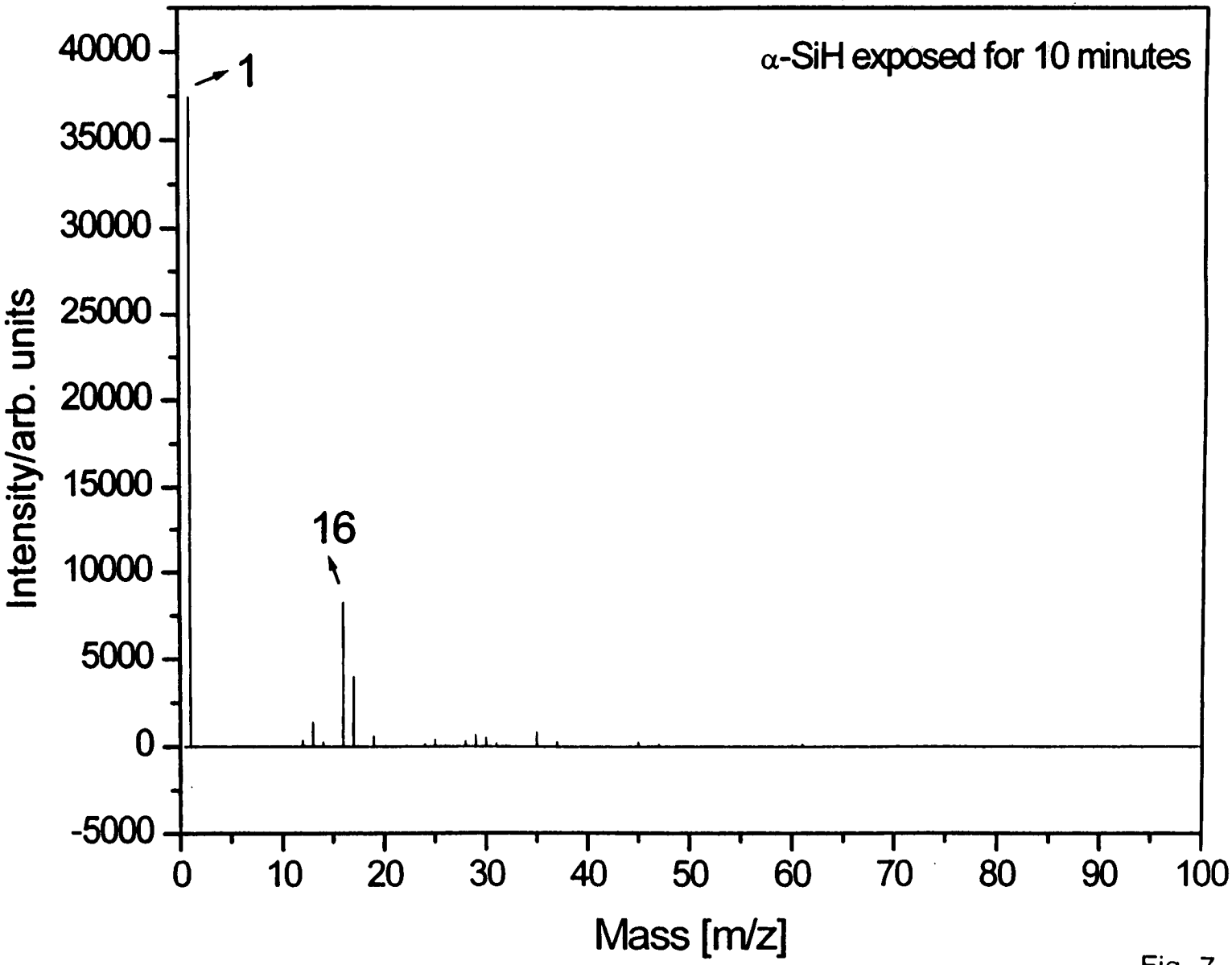
α-SiH exposed for 10 minutes
1
16
Intensity/arb. units
40000
35000
30000
25000
20000
15000
10000
5000
0
-5000
0
10
20
30
40
50
60
70
80
90
100
Mass [m/z]

Fig. 7

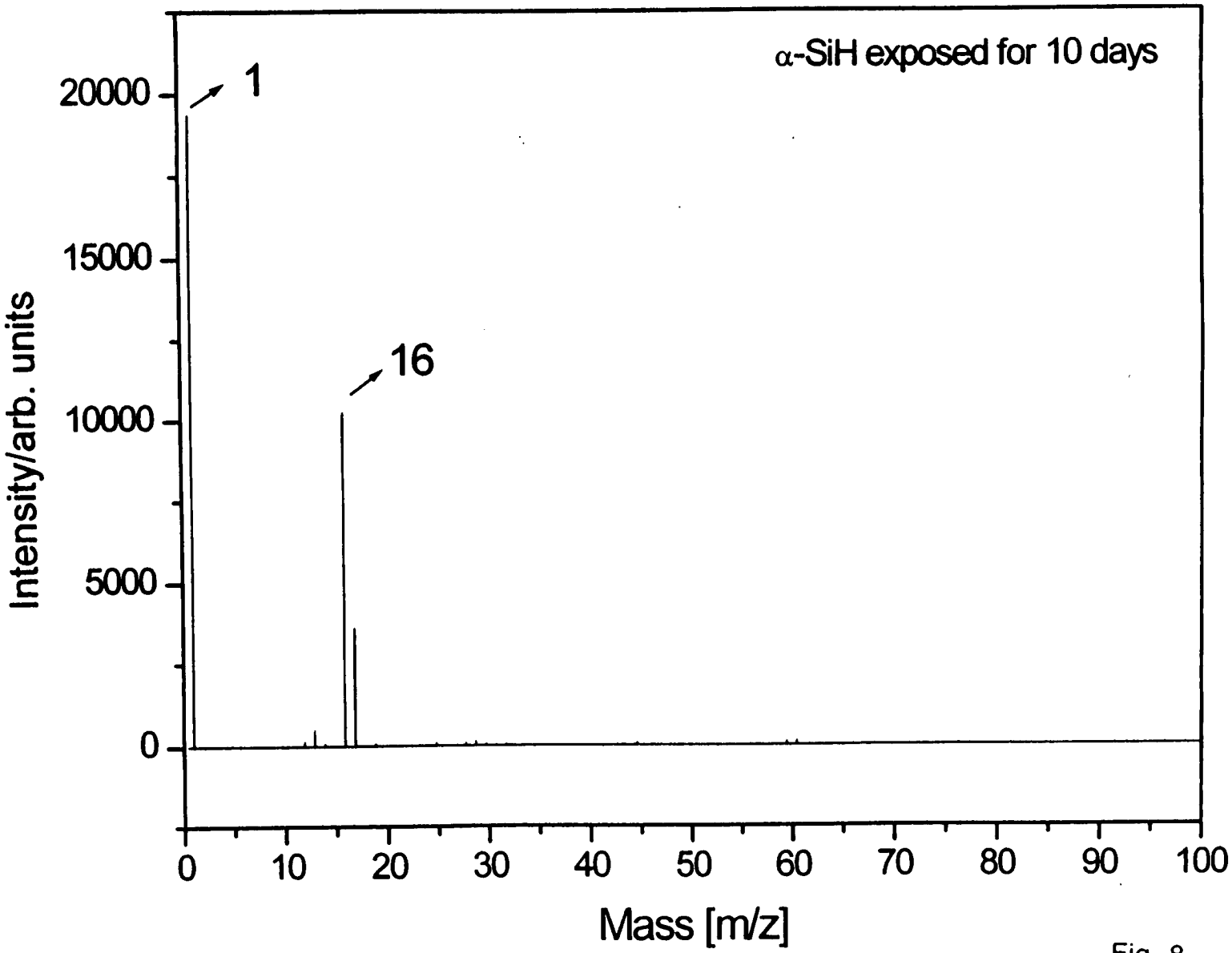
α-SiH exposed for 10 days
1
16
20000
15000
10000
5000
0
Intensity/arb. units
0
10
20
30
40
50
60
70
80
90
100
Mass [m/z]

Fig. 8

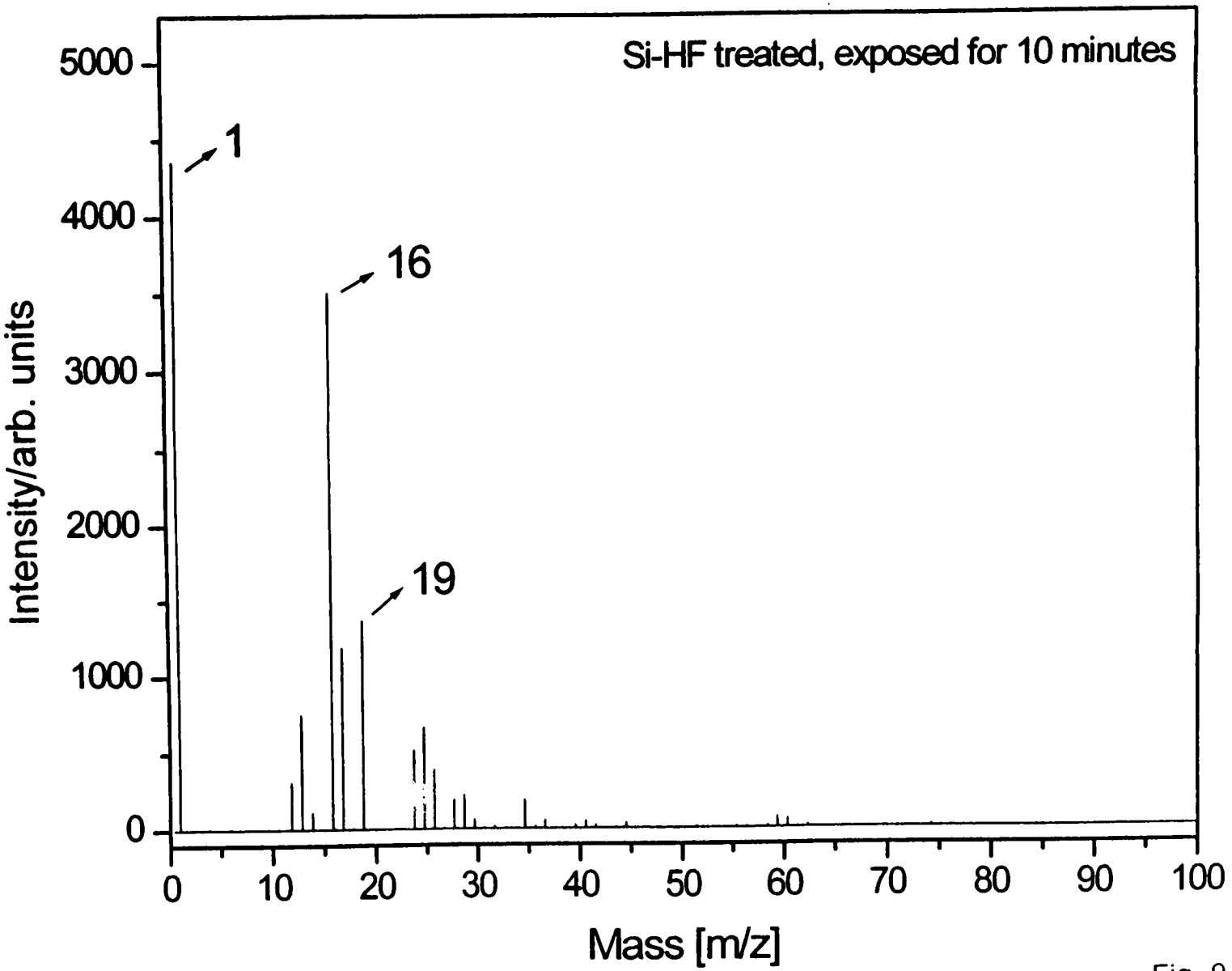
Si-HF treated, exposed for 10 minutes
Intensity/arb. units
Mass [m/z]
1
16
19
0
1000
2000
3000
4000
5000
0
10
20
30
40
50
60
70
80
90
100

Fig. 9

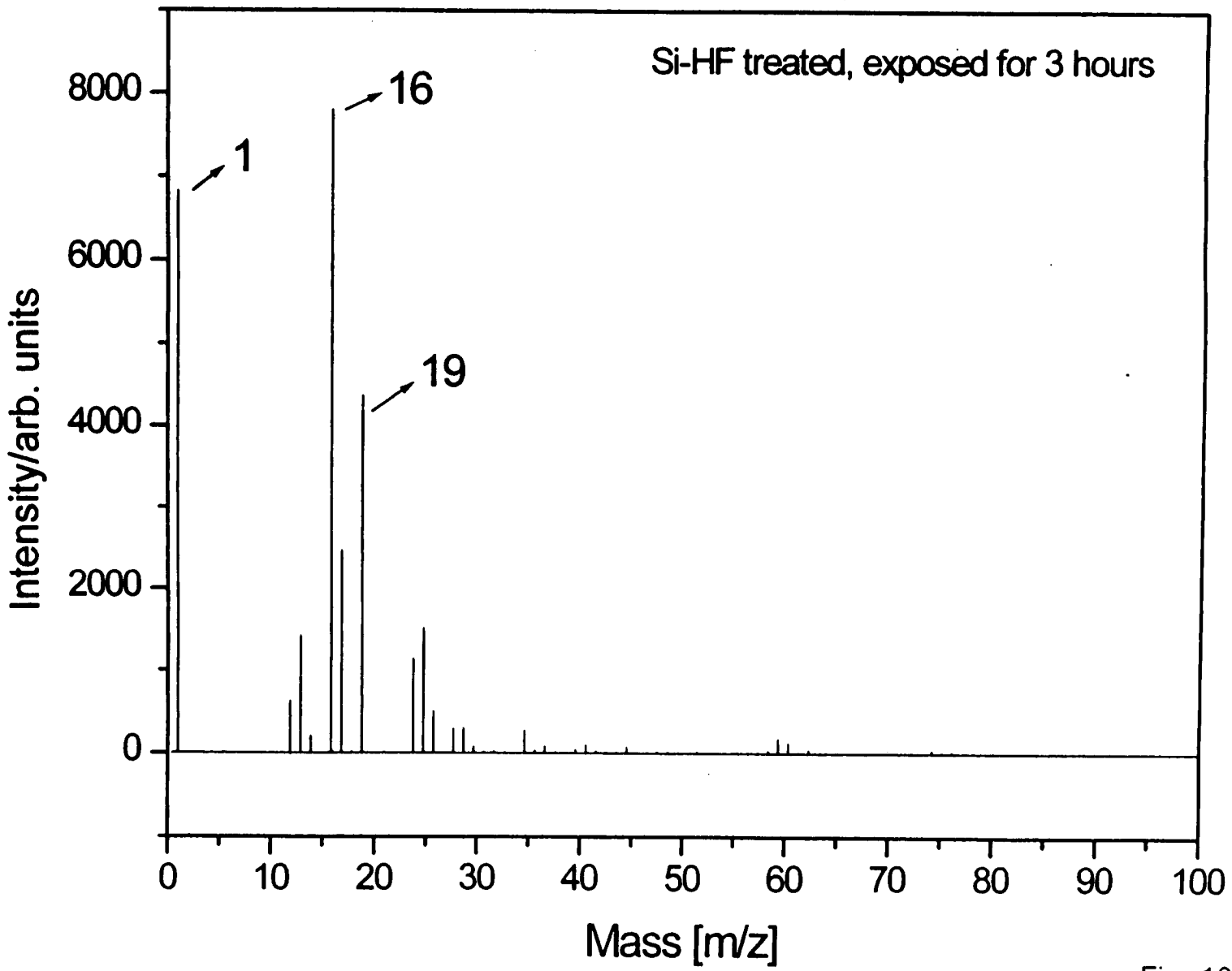
Si-HF treated, exposed for 3 hours
16
1
19
8000
6000
4000
2000
0
Intensity/arb. units
0
10
20
30
40
50
60
70
80
90
100
Mass [m/z]

Fig. 10

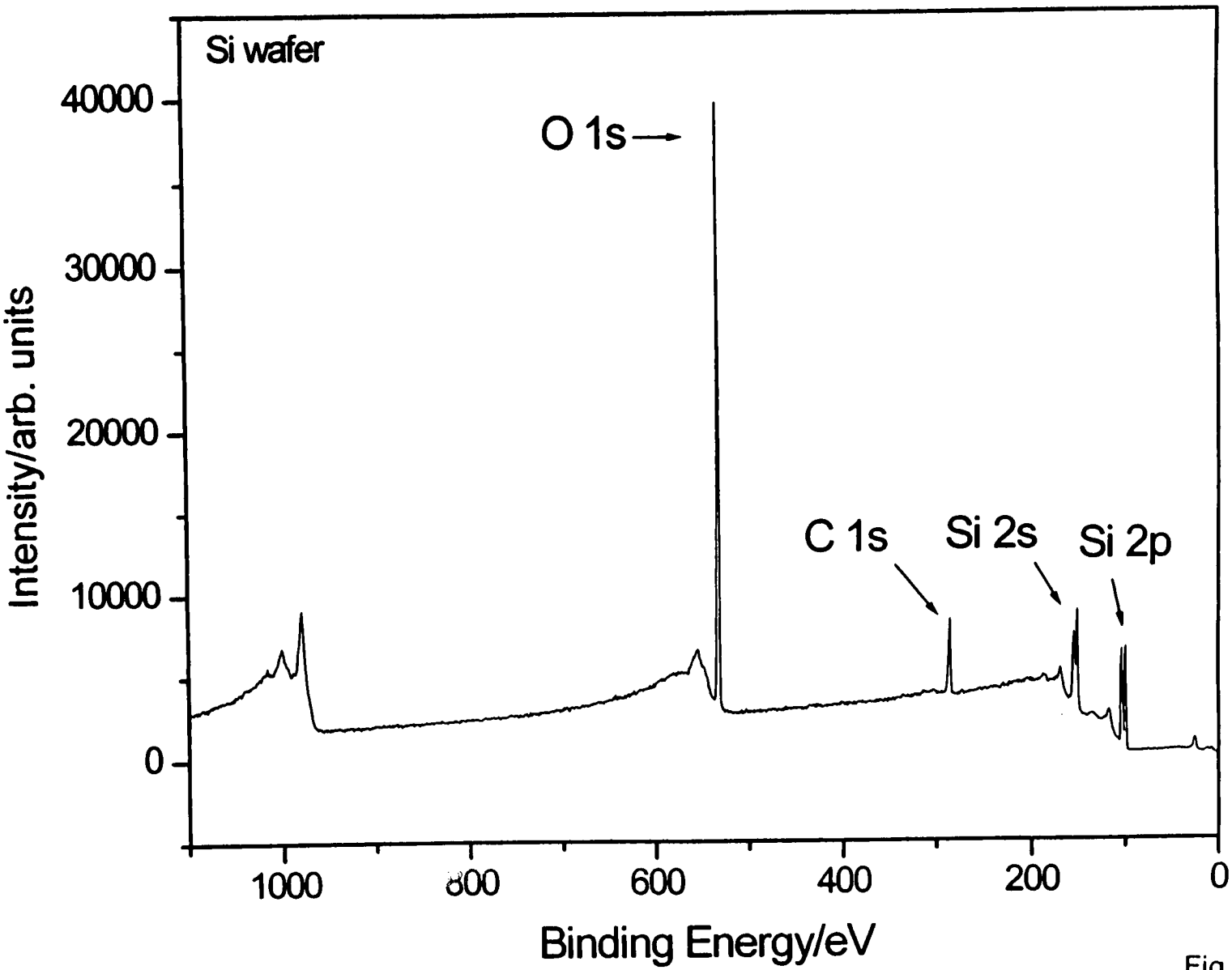
Si wafer
O 1s
C 1s
Si 2s
Si 2p
Intensity/arb. units
40000
30000
20000
10000
0
1000
800
600
400
200
0
Binding Energy/eV

Fig. 11

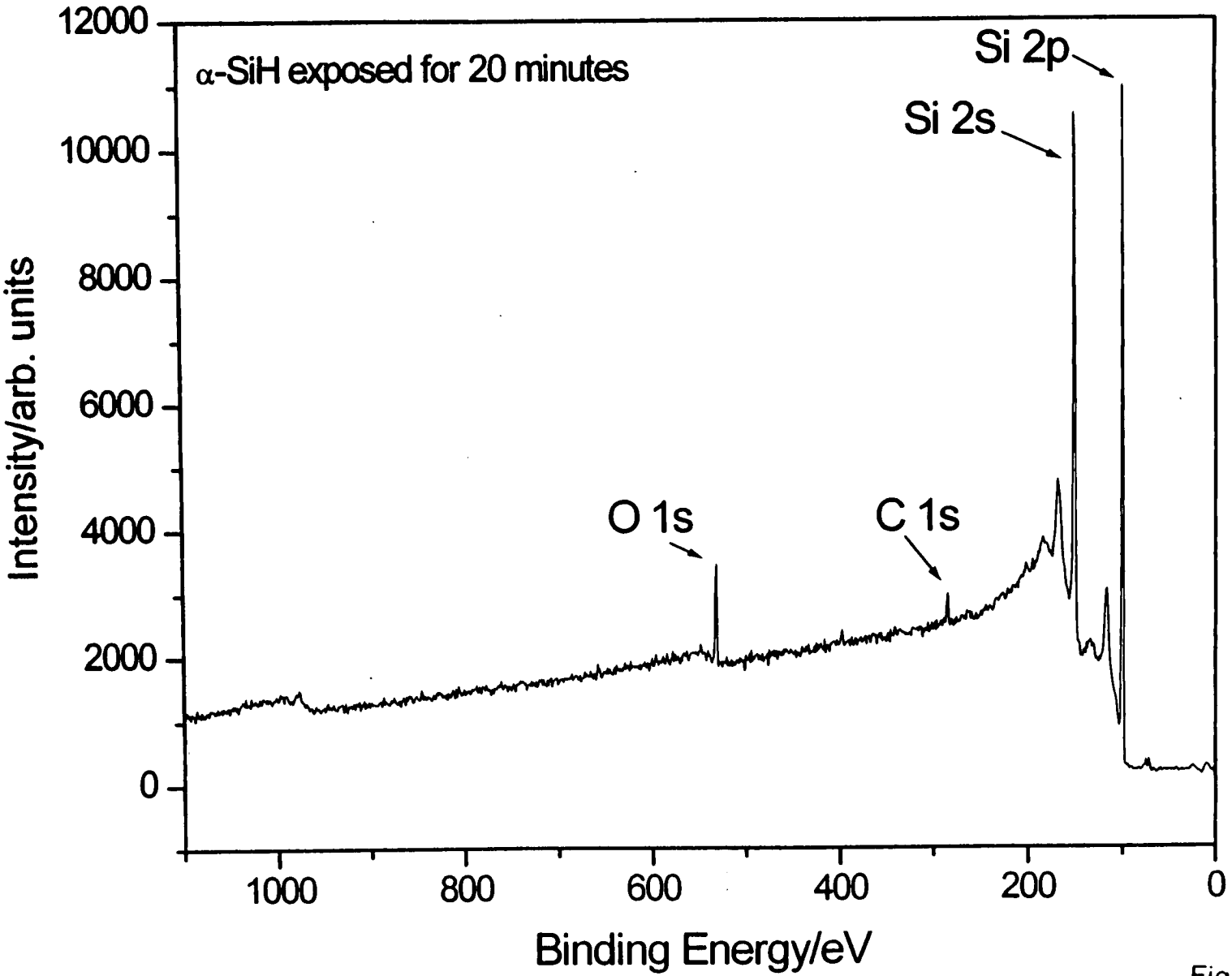
α-SiH exposed for 20 minutes
Si 2p
Si 2s
O 1s
C 1s
Intensity/arb. units
12000
10000
8000
6000
4000
2000
0
1000
800
600
400
200
0
Binding Energy/eV

Fig. 12

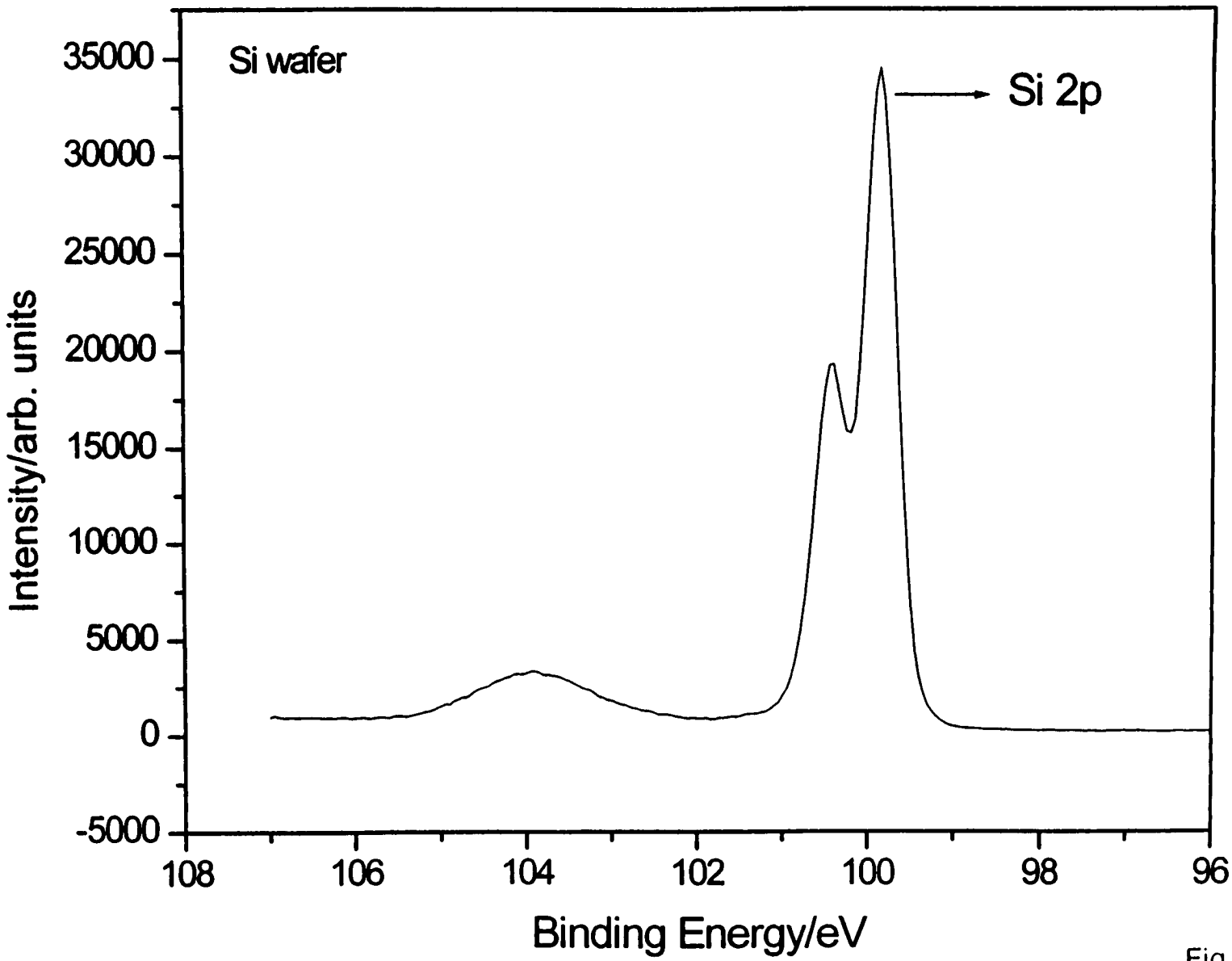
Si wafer
Si 2p
35000
30000
25000
20000
15000
10000
5000
0
-5000
Intensity/arb. units
108
106
104
102
100
98
96
Binding Energy/eV

Fig. 13

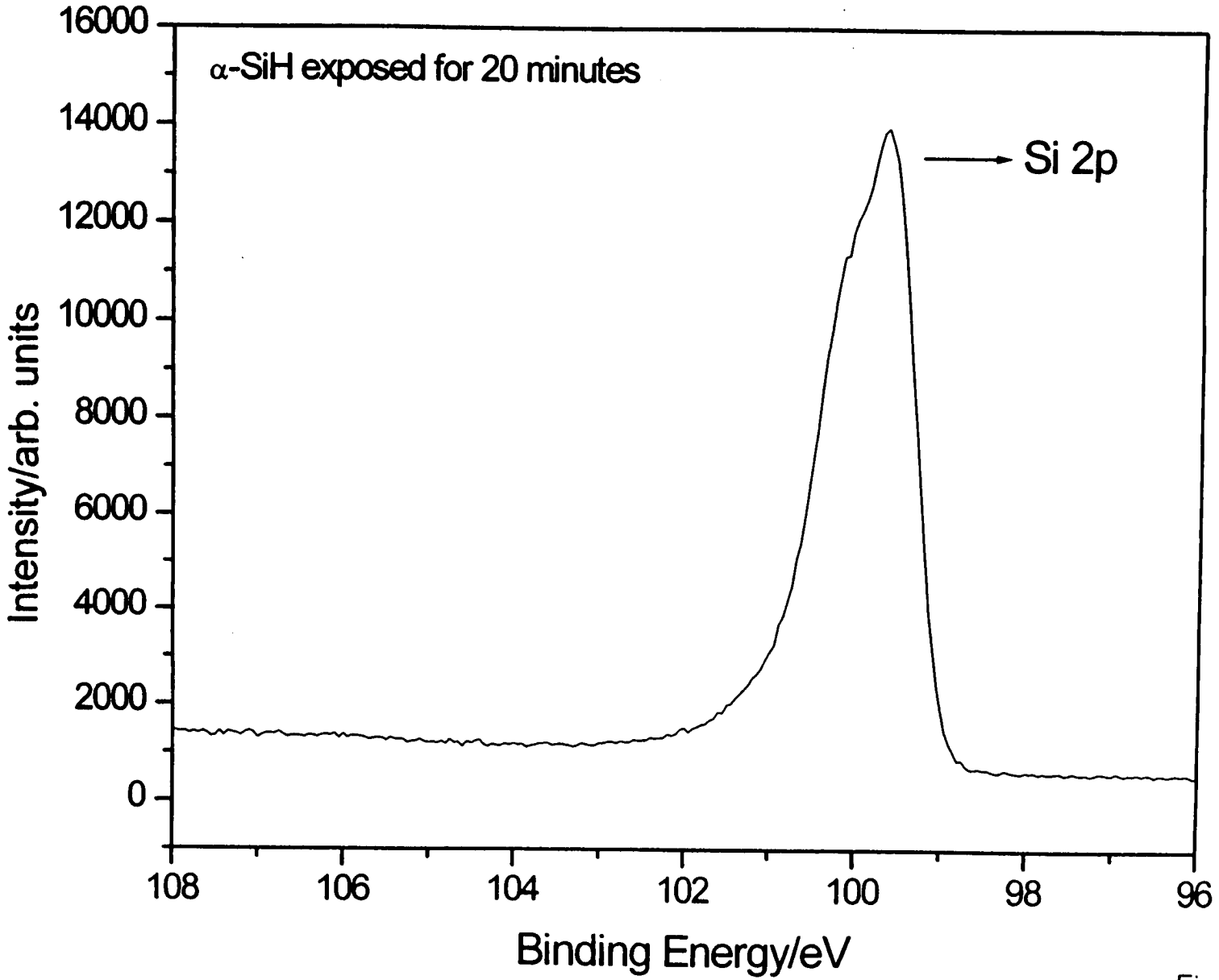
α-SiH exposed for 20 minutes
Si 2p
Intensity/arb. units
16000
14000
12000
10000
8000
6000
4000
2000
0
108
106
104
102
100
98
96
Binding Energy/eV

Fig. 14

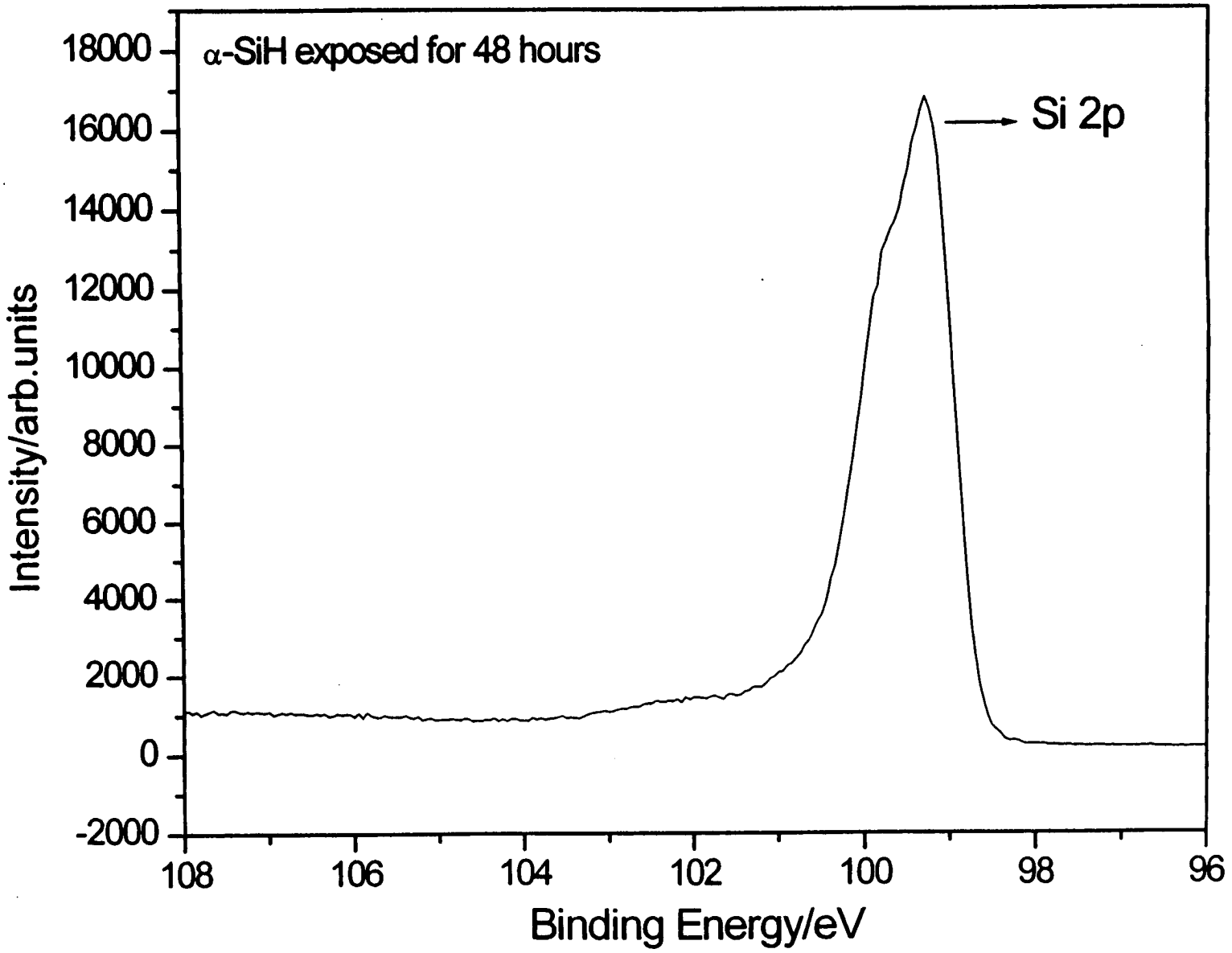
α-SiH exposed for 48 hours
Si 2p
Intensity/arb.units
18000
16000
14000
12000
10000
8000
6000
4000
2000
0
-2000
108
106
104
102
100
98
96
Binding Energy/eV

Fig. 15

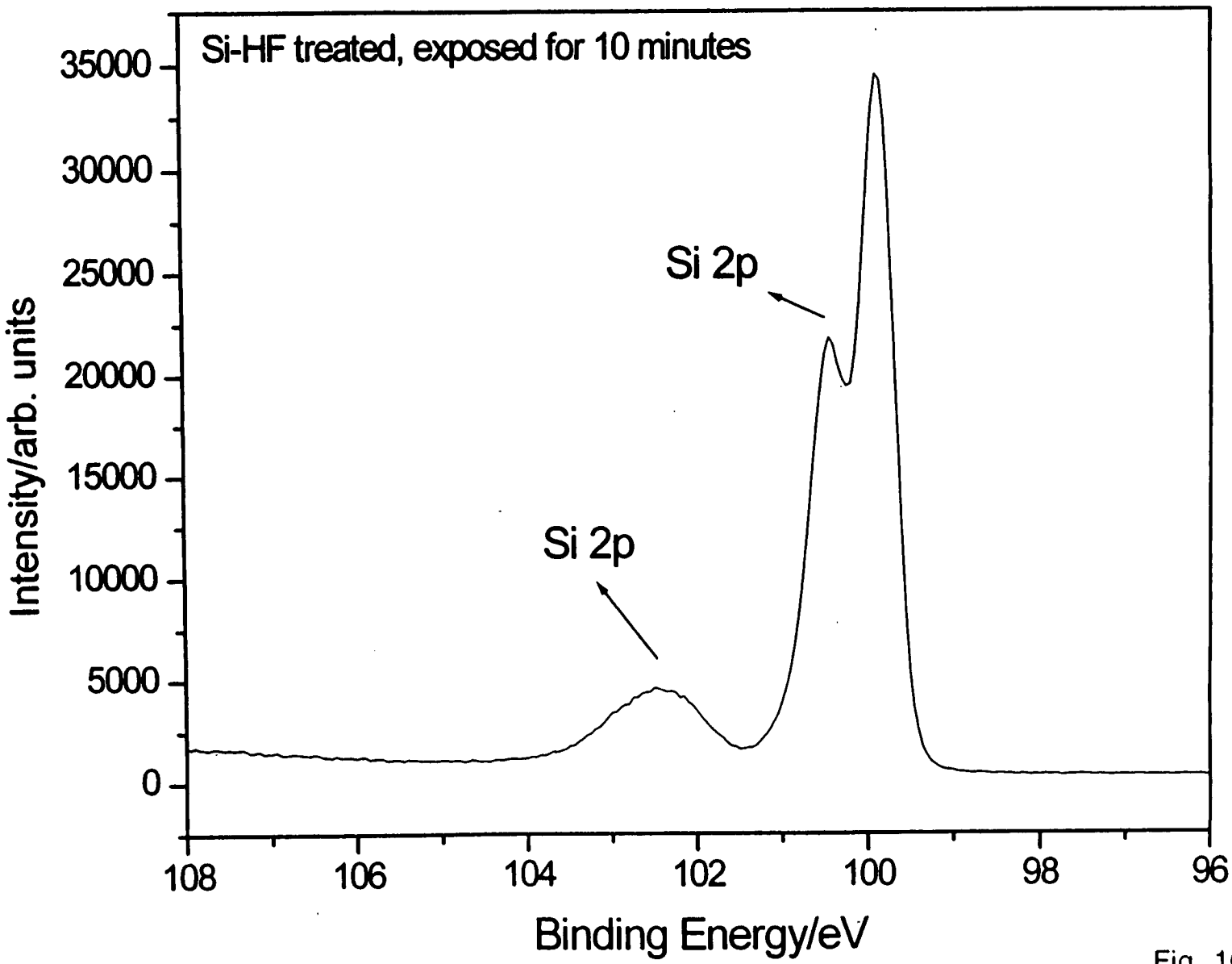
Si-HF treated, exposed for 10 minutes
Si 2p
Si 2p
Intensity/arb. units
35000
30000
25000
20000
15000
10000
5000
0
108
106
104
102
100
98
96
Binding Energy/eV

Fig. 16

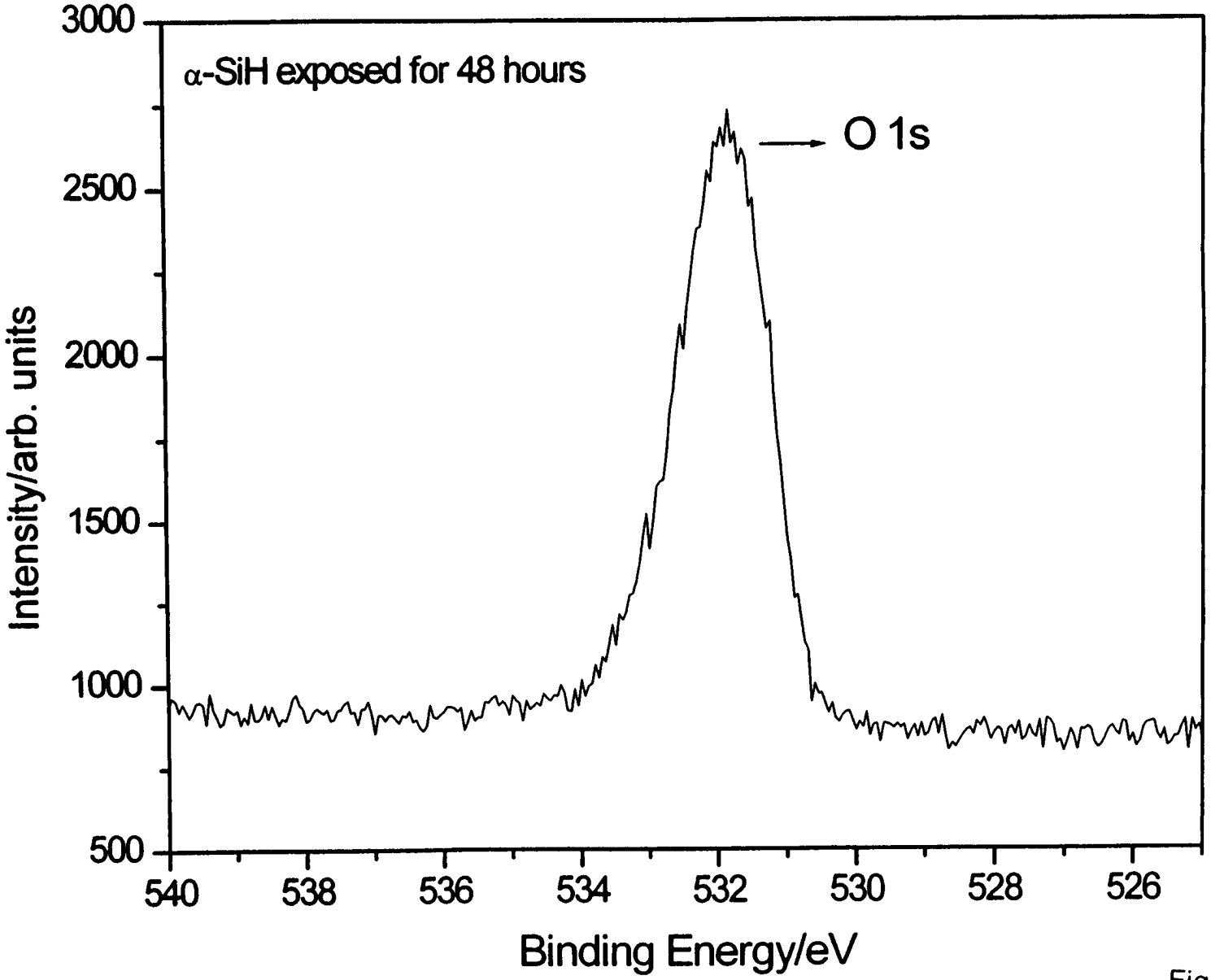
α-SiH exposed for 48 hours
O 1s
Intensity/arb. units
3000
2500
2000
1500
1000
500
540
538
536
534
532
530
528
526
Binding Energy/eV

Fig. 17

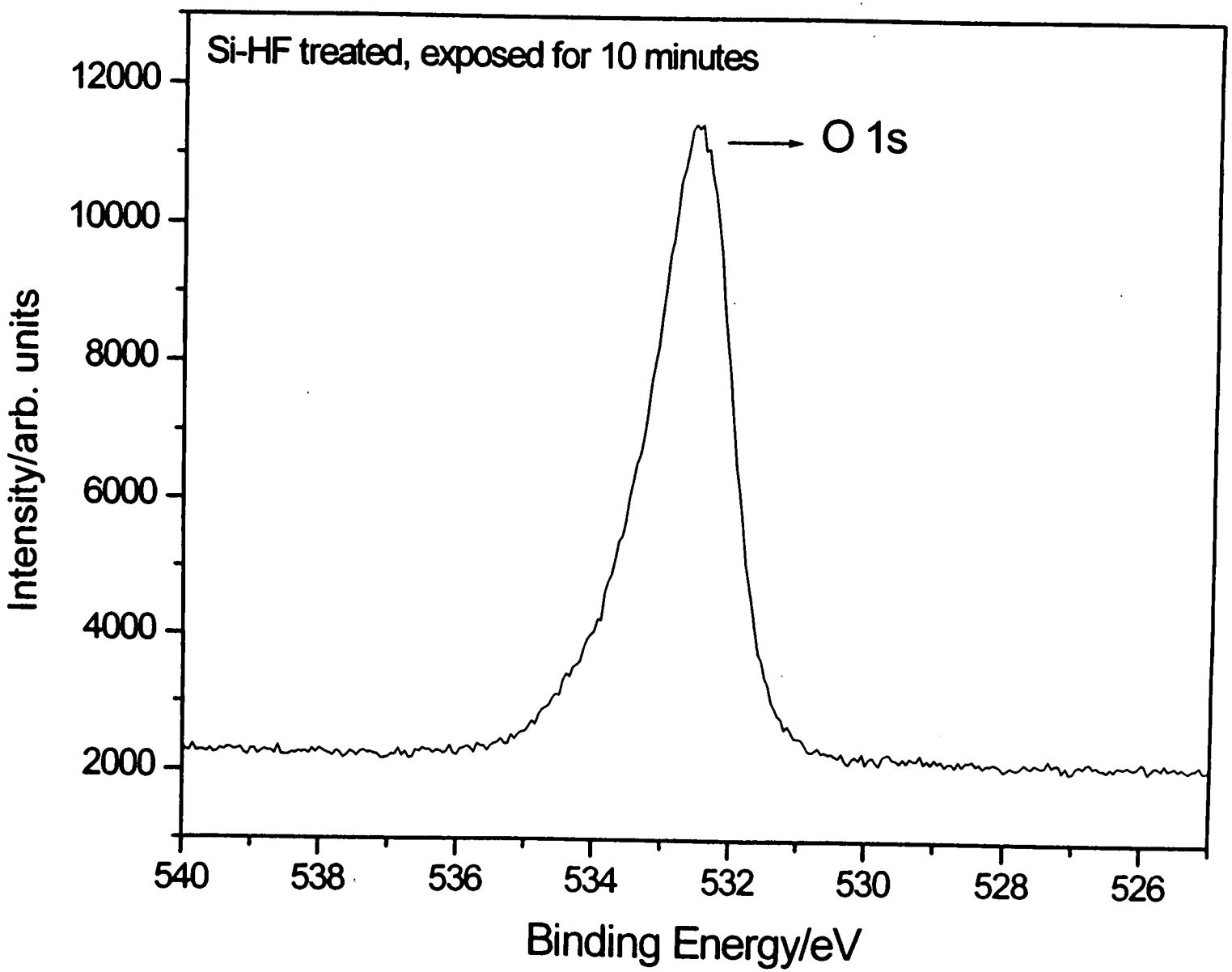
Si-HF treated, exposed for 10 minutes
O 1s
12000
10000
8000
6000
4000
2000
Intensity/arb. units
540
538
536
534
532
530
528
526
Binding Energy/eV

Fig. 18

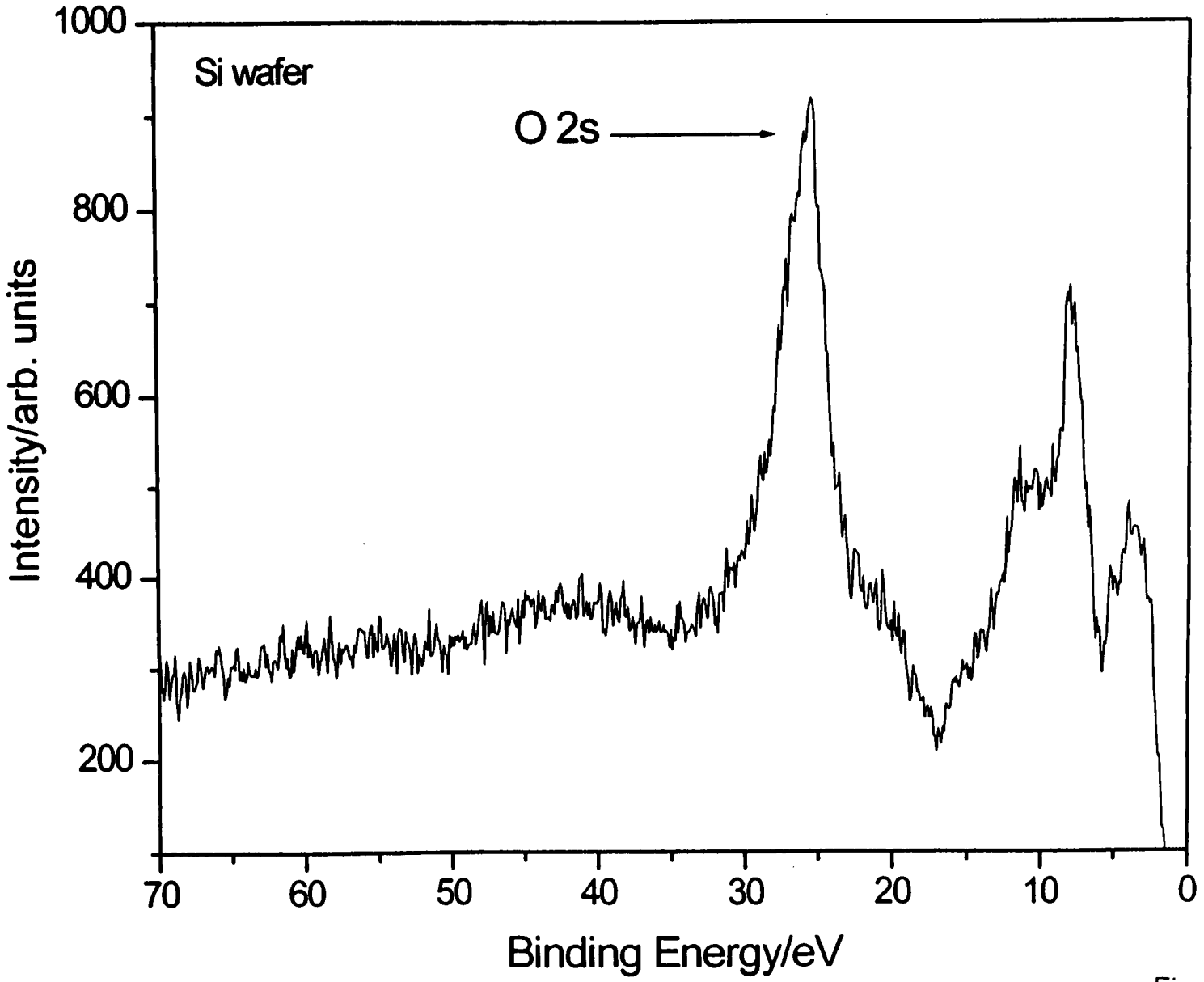
Si wafer
O 2s
Intensity/arb. units
1000
800
600
400
200
70
60
50
40
30
20
10
0
Binding Energy/eV

Fig. 19

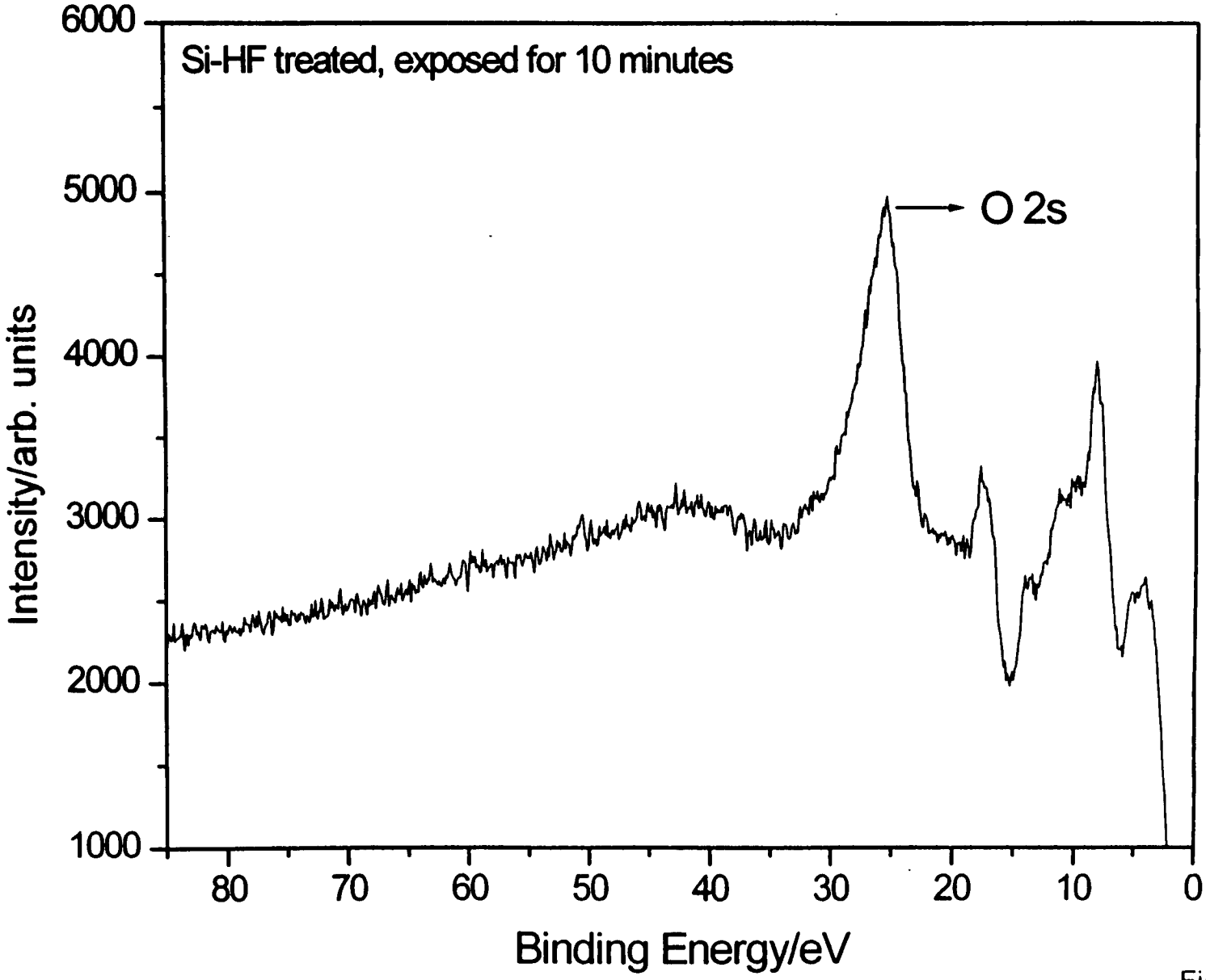
Si-HF treated, exposed for 10 minutes
O 2s
Intensity/arb. units
6000
5000
4000
3000
2000
1000
80
70
60
50
40
30
20
10
0
Binding Energy/eV

Fig. 20

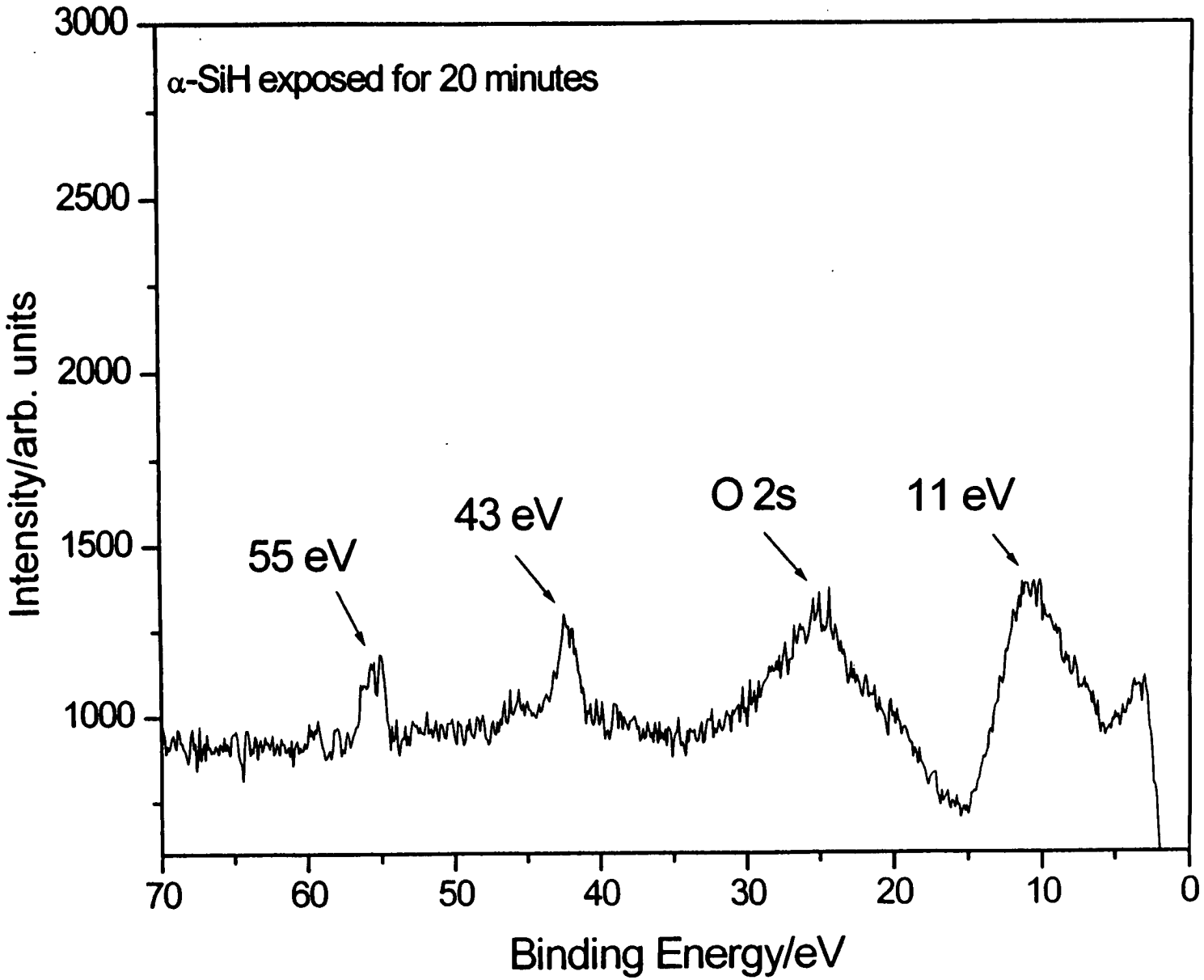
α-SiH exposed for 20 minutes
Intensity/arb. units
3000
2500
2000
1500
1000
55 eV
43 eV
O 2s
11 eV
70
60
50
40
30
20
10
0
Binding Energy/eV

Fig. 21